1975

Determination Of Absorption And Atomic Number Corrections In Electron Probe Microanalysis For Electron Energies Below 15 Kev

Lubomir Parobek

DETERMINATION OF ABSORPTION AND ATOMIC NUMBER CORRECTIONS IN ELECTRON PROBE MICROANALYSIS FOR ELECTRON ENERGIES BELOW 15 keV

by

Lubomir Parobek

Department of Engineering Science

Submitted in partial fulfillment
of the requirements for the degree of
Doctor of Philosophy

Faculty of Graduate Studies
The University of Western Ontario
London, Canada

May 1975

ABSTRACT

Using sandwich samples which consist of a layer of identical thickness of a single tracer element deposited within sandwich samples having a different atomic number of the matrix element, the depth distributions of the x-ray production, $\phi(\rho z)$ curves, were measured for SiKα radiation for 6, 8 and 10keV in Al, Ni, Ag and Au matrices and for CuKα radiation for 12 and 15 keV in Al, Ni and Ag matrices. The electron beam was normal to the surface of the specimen. From these curves, absorption [$f(\chi)$] and atomic number corrections were derived.

The $f(\chi)$ values calculated according to Philibert formula were compared to the $f(\chi)$ values calculated from the measured $\phi(\rho z)$ curves. The atomic number correction factors for SiKα radiation obtained as ratios of an area under $\phi(\rho z)$ curves for Ni, Ag and Au matrices to the area under $\phi(\rho z)$ curve for Al matrix, respectively, and atomic number correction factors for CuKα radiation obtained as ratios of an area under $\phi(\rho z)$ curves for Al and Ag matrices to the area under $\phi(\rho z)$ curve for Ni matrix, respectively, were compared to equivalent factors calculated from the Duncumb and Reed method and the Diffusion model.

An expression of the form

$$\phi(R) = DnK\ (KR)^{n-1} \exp\ [-(KR)^{n}]$$

which describes the depth distribution of the x-ray production has been generated. The parameters in this expression depend on, the energy of electrons, the critical excitation energy and average atomic weight and atomic number of the matrix. With the aid of this function a new correction for absorption and atomic number, for electron energies below 15keV was developed and was shown to give better results in quantitative analysis on data from standards of known composition reported in the literature.

ACKNOWLEDGEMENTS

The author wishes to express his sincere appreciation for the encouragement and guidance of Dr. J.D. Brown of the University of Western Ontario

To his wife he expresses deep gratitude for her patience and understanding throughout the duration of his studies.

He would like to thank Dr. L.N. Johnson, Faculty of Dentistry, University of Western Ontario, whose co-operation made possible the measurements of depth distribution curves.

I would like to thank the National Research Council of Canada for their financial support during the period of my studies at the University of Western Ontario.

TABLE OF CONTENTS

INTRODUCTION

The electron probe microanalyzer is used in research, development, and quality control in such diverse scientific areas as metallurgy, mineralogy, criminology, biochemistry, pathology, zoology, physics and electronics. While the instrument has made its greatest impact in the study of materials and minerals, its use in other areas is rapidly expanding and the technique holds particular promise in the areas of biology and environmental science.

In the electron probe microanalyzer a beam of electrons from an electron gun is accelerated by a potential of few to 50 kilovolts, then focused by means of magnetic lenses to a spot of the order of one micron in diameter at the surface of a specimen. These electrons excite the atoms in a small volume of the specimen by removal of electrons from the inner (K, L, or M) shells. In returning to the ground state these atoms emit x-rays whose energies are characteristic of the atomic number of the excited atoms. Because the electrons can penetrate to a distance of a few microns in the specimen, the x-rays are generated within the specimen as well as at the surface. The value of the instrument lies in its ability to generate a measurable x-ray intensity in extremely small volumes of material, approaching one cubic micrometer, to identify all elements with atomic number greater than three, and, in many cases to provide a quantitative chemical analysis.

LIST OF TABLES

LIST OF FIGURES

NOMENCLATURE

I_{AB}, I_A	=	The intensities of the characteristic x-ray line of the element A emitted from the specimen and pure element standard, respectively.
I'_{AB}, I'_A	=	The intensities of the characteristic x-ray line of the element A generated in the specimen and standard, respectively.
C_A	=	Mass concentration of element A.
Z	=	Depth below sample surface.
ρz	=	Mass depth.
ρ	=	Density.
$\phi(\rho z)$	=	Depth distribution of the x-ray production.
χ	=	$\mu \csc \psi$
μ	=	Mass absorption coefficient.
ψ	=	X-ray take-off angle.
ϕ_i	=	The angle between the normal to the surface of the specimen and the electron path in the specimen.
N_A	=	Avagadro's number.
e	=	Charge of electron or base of natural logaritms.
A_A	=	Atomic weight of element A.
Z_A	=	Atomic number of element A.
$F(\chi)$	=	Laplace transform of $\phi(\rho z)$.
$f(\chi)$	=	Philibert's absorption factor.
K_F	=	Fluorescence correction due to the characteristic lines.

σ	=	Lenard coefficient.
k	=	Parameter reflecting the variation in the amount of electron scattering with atomic number in Philibert's work (equation [1-13]).
h	=	σ/k
K_A	=	I_{AB}/I_A
α_A, α_B	=	Empirical terms introduce by Castaing to produce atomic number correction.
Θ	=	Scattering angle with respect to initial direction of electrons.
s	=	Distance along electron path.
Q_A	=	Ionization cross-section for shell of element A.
ω_A	=	Fluorescent yield.
P_{i_A}	=	Probability of emission of the specific spectral line.
$N_o(z)$	=	Number of electrons striking a unit area of the target at a depth z.
E_o	=	Energy of incident electrons.
E_c	=	Critical excitation energy.
R	=	Back scattering factor.
$-S$	=	Stopping power.
J	=	Mean ionization potential.
α	=	Screening factor (equation 3-14).
$\sigma(\Theta)$	=	Rutherford cross section.
$R(\rho z)$	=	Philibert's all-inclusive scattering function.
R_o, R_∞	=	Values of $R(\rho z)$ at the surface of the target and at the depth of complete diffusion of the electrons, respectively.

n_K	=	The total number of ionizations of the K-shell.
N_T	=	Total number of counts.
S_T	=	Standard deviation for total number of counts.
N_B	=	Number of background counts.
S_B	=	Standard deviation for background counts.
S_ϕ	=	standard deviation in the determination of value of $\phi(\rho z)$.

INTRODUCTION

The electron probe microanalyzer is used in research, development, and quality control in such diverse scientific areas as metallurgy, mineralogy, criminology, biochemistry, pathology, zoology, physics and electronics. While the instrument has made its greatest impact in the study of materials and minerals, its use in other areas is rapidly expanding and the technique holds particular promise in the areas of biology and environmental science.

In the electron probe microanalyzer a beam of electrons from an electron gun is accelerated by a potential of few to 50 kilovolts, then focused by means of magnetic lenses to a spot of the order of one micron in diameter at the surface of a specimen. These electrons excite the atoms in a small volume of the specimen by removal of electrons from the inner (K, L, or M) shells. In returning to the ground state these atoms emit x-rays whose energies are characteristic of the atomic number of the excited atoms. Because the electrons can penetrate to a distance of a few microns in the specimen, the x-rays are generated within the specimen as well as at the surface. The value of the instrument lies in its ability to generate a measurable x-ray intensity in extremely small volumes of material, approaching one cubic micrometer, to identify all elements with atomic number greater than three, and, in many cases to provide a quantitative chemical analysis.

For quantitative analysis, the x-ray intensity of a characteristic line for each element must be related to the composition. Castaing [1] demonstrated that the relationship between the mass concentration C_A of an element A in a specimen analyzed in the electron microprobe, and the ratio I_{AB}/I_A of the intensity of the characteristic x-ray line from the specimen to that from a standard consisting of the pure element, A, is to a first approximation, simply

$$C_A = \frac{I_{AB}}{I_A} \qquad (1)$$

Instrumental corrections such as those for dead-time and background are carried out before calculating I_{AB}/I_A, and the intensities from specimen and standard are measured under identical experimental conditions. Departures from the simple law of proportionality expressed in Equation (1) can be large, and if accurate quantitative analysis is to be attempted with the electron microprobe, it is essential to apply a correction factor

$$\frac{I_{AB}}{I_A} = C_A \times (\text{correction factor})$$

The correction factor is placed on the right hand side of the equation because it is itself a function of C_A, and of the concentrations of the other elements present.

Castaing's simple approximation (Eqn. 1) applies to the intensities which are generated by the electrons inside the specimen.

Experimentally, the intensities cannot be measured since x-rays emerging from the specimen (unknown) will be absorbed in reaching the specimen surface. The amount of absorption will be different in the unknown and in the standard. Procedures for the correction of these differential absorption effects have been pursued by Castaing [1], Castaing and Descamps [2] and Philibert [3]. In addition, the measured x-ray intensities may also include contributions from secondary emission (fluorescence) caused by absorption of higher energy characteristic radiation generated in atoms of the specimen by the electron beam or by the higher energy portion of the continuous spectrum. Procedures for correction of fluorescence effects have been given by Castaing [1], Wittry [4,5], Duncumb and Shields [6], Henoc [7], Birks [9], Reed [8], and J.D. Brown [10].

Even in the absence of fluorescence effects, the simple expression which states that the x-ray intensity directly excited by electrons is proportioned to the concentration is inexact because the stopping power and back-scatter fraction for electrons varies from element to element. Because of these phenomena both the number of x-rays generated and the distribution of x-rays generated as a function of depth will vary in targets of different

average atomic number. The phenomena collectively make up the atomic number effect. To get the true concentration of the element in the unknown, a correction factor has to be introduced. Many authors, Castaing [11], Archard and Mulvey [12], Theisen [14], Birks [9], Thomas [16], Ziebold and Ogilvie [13], Poole and Thomas [17], and Belk [18] have attempted to evaluate this correction. Both empirical and theoretical models have been used to evaluate the atomic number correction. The empirical approach is based on comparing predicted and measured intensities from a large number of standards and modifying the correction equation by adjustable parameters.

The theoretical approaches (Diffusion Model, Monte Carlo calculation, Transport Equation) to establish the correction factors use physical data on the interaction of electrons and matter. Both theoretical and empirical approaches would benefit from independent data as a guide to the appropriateness of the models and for comparison of the results. Measurements of x-ray production by electrons as a function of depth in a specimen ($\phi(\rho z)$ curves) can provide these independent experimental data. At electron energies higher than 15 keV such $\phi(\rho z)$ curves have been measured by many authors [2], [10], [19], [11], [34], [35]. No measurements have been made for electron energies below 12 keV. The purpose of this thesis is to provide experimental data of the depth distribution at electron energies from 6 to 15 keV.

As electron energy decreases the volume of the material excited by the electrons sharply decreases. Thus, the information about chemical composition obtained by using these low electron energies will be from extremely small volumes. This is most important in cases where the composition of the material examined is sharply changing with depth, for example in case of inclusions or precipitates. Unfortunately the correction factors for these low energies have been extrapolated from data at high energies. The need for more reliable absorption and atomic number corrections is obvious.

The electron interaction with solids has been studied at least for 40 years. But most of the relationships, as mentioned above, have been obtained either by experiments with a high-energy beam or by theoretical considerations under assumptions which are also applicable only at high energies. It can be shown that the intensity of characteristic x-rays generated in the solid specimen, I_A, is

$$I_A = \text{const.}\ C_A\ R \int_{E_C}^{E_0} (Q/S)\ dE \qquad (2)$$

where C_A is weight concentration of the element A in the volume excited, R is backscatter coefficient (equal to the ratio of the intensity actually generated to that which would be generated if all the incident electrons stayed in the specimen), Q is the ionization cross-section (is defined as the probability per unit path length of an

electron with a given energy causing ionization of a particular inner electron shell (K, L or M) of an atom in the specimen), S is the stopping power (the ability of a given material to slow down incident electrons), E_o is the energy of the incident electrons and E_c is the critical excitation potential.

The R values used in most atomic number corrections have been determined from the values of the electron backscattering coefficients, η, measured at 20 keV. Thus, for example, for heavy elements in combination with light elements and at electron energies much lower than 20 keV the error in the correction factor is more than ± 20%. The most used formula for stopping power is that given by Bethe

$$S = \text{const.}\ (Z/A)\ (1/E)\ \ln\ (1.166\ E/J) \qquad (3)$$

where Z and A are respectively the atomic number and atomic weight of the element concerned and J is mean ionization potential.

When a stream of electrons penetrates into a solid target, electrons may be scattered either elastically or inelastically. Electron stopping power is due to inelastic collisions with atomic electrons and it is actually a discrete loss of energy while stopping power expressed by Eq. (3) represents continuous loss of energy. For elements of high atomic numbers and at high electron energies this approximation agrees well with experiment but the validity of this expression is quite questionable at

low electron energies and for elements of low atomic number.

Due to the complex calculations and uncertainties involved in applying correction formulae, some investigators prefer to use a comparison method based on calibration standards to determine compositions of samples [17]. Although this method may be useful in some cases, its application is limited by the availability of homogeneous standards whose compositions are accurately known. Furthermore, the full potential of quantitative analysis by x-ray emission spectrometry is not realized.

CHAPTER I

The Physical Basis of Quantitative Analysis

The absolute method of quantitative chemical analysis is based, as was already mentioned in the Introduction, on the comparison of measured intensities of the same characteristic radiation from an unknown I_{AB} and from a pure element standard, I_A, thus

$$C_A = \frac{I_{AB}}{I_A}$$

where C_A is the weight fraction of the element A in the AB system.

This simple ratio of the two intensities gives to a first approximation the concentration of an element A in the unknown. However, the simple ratio I_{AB}/I_A does not yield true concentration of the element A in the unknown for all samples and corrections must be applied to the measured intensities.

The physical basis of the corrections which must be applied to the measured intensities for the quantitative determination of the composition of microvolumes was outlined by Castaing [1]. Castaing [2] has shown that the intensity generated in a thin layer $d(\rho z)$ at a depth ρz in a pure element A can be expressed by the following:

$$dI_A = \phi(\rho z)\, d(\rho z) \qquad (1\text{-}1)$$

where $\phi(\rho z)$ usually taken as the ratio of intensity from a thin layer in the sample to the intensity from a layer of the same thickness isolated in space. $\phi(\rho z)$ therefore represents the characteristic x-ray distribution with depth. If equation (1-1) is integrated from the surface of the specimen to an infinite thickness, we obtain the expression for the total x-ray intensity generated in the sample.

$$I_A = \int_0^\infty \phi(\rho z)\, d(\rho z) \equiv F(0)_A \qquad (1\text{-}2)$$

This expression for the generated x-ray intensity must be corrected for absorption of the x-rays on leaving the sample to correspond to the intensity measured by the spectrometer. If we include absorption, the intensity I_A escaping from the sample is

$$I_A = \int_0^\infty \phi(\rho z) \exp\{-[\mu\, \rho z \csc \psi]\}\, d(\rho z) \equiv F(\chi)_A \qquad (1\text{-}3)$$

where μ is the mass absorption coefficient of the specimen for the radiation of interest from element A, ψ is the x-ray take-off angle, $\chi = \mu \csc \psi$ and $F(\chi)_A$ is the Laplace transform of $\phi(\rho z)$. For an alloy AB, the equation (1-3) becomes

$$I_{AB} = C_A\, F(\chi)_{AB} \qquad (1\text{-}4)$$

where C_A is the weight fraction of element A in the alloy AB. By taking the ratio of equations (1-4) and (1-3) we obtain the expression

$$K_A \equiv \frac{I_{AB}}{I_A} = C_A \frac{f(\chi)_{AB}}{f(\chi)_A} \frac{F(0)_{AB}}{F(0)_A} \qquad (1\text{-}5)$$

where

$$f(\chi) = \frac{F(\chi)}{F(0)}$$

Equation (1-5) is applicable only in the absence of fluorescence effects.

Castaing assumed for his first approximation that the mass concentration, C_A, of the element A in the unknown is equal

$$C_A = \frac{I_{AB}}{I_A} \frac{f(\chi)_A}{f(\chi)_{AB}} \qquad (1\text{-}6)$$

which is equivalent to equation (1-5) assuming that $F(0)_{AB}/F(0)_A$ is equal to 1, i.e., that the x-ray intensity generated in the sample per atom of element A, is the same in both pure element and unknown. However, experimental and theoretical evidence indicates that this is not so for matrices of different average atomic numbers. This is the origin of the atomic number effect. The simple equation (1-6) must then be modified to

$$K_A = C_A \frac{f(\chi)_{AB}}{f(\chi)_A} \alpha$$

where α is atomic number correction factor, to take into account this atomic number effect.

When the wavelength of a characteristic line of one element in a sample falls on the short wavelength side of an absorption edge of a second element in the sample, then fluorescence of the second element occurs. In extreme cases the contribution due to fluorescence can increase the observed x-ray intensity from an element in the sample by more than 50 percent. If characteristic fluorescence is important then equation (1-6) must be modified to

$$K_A = C_A \frac{f(\chi)_{AB}}{f(\chi)_A} \alpha(1 + K_F)$$

where K_F is the fluorescence correction.

X-rays are also generated when the incident electrons are deflected due to close approach to other electrons and the atomic nuclei in the target. These x-rays, however, have a continuous range of energies from very low energies up to a maximum which is equivalent to the electron energy. The x-rays generated by this mechanism are termed the continuum. All wavelengths of the continuum which are of greater energy than the absorption edge energy of an element in the sample can contribute to fluorescence of that element. The magnitude of the intensity of characteristic x-rays from an element due to fluorescence by the continuum can be as great as seven or eight percent of the intensity directly excited by electrons. Additional terms must be

added to K_F to account for continuum fluorescence.

A fundamental method for determining the magnitude of the corrections is to find the distribution of x-ray production with depth, $\phi(\rho z)$. This has been determined experimentally in 1955 by Castaing and Descamps [2] and has been derived theoretically in 1963 by Philibert [3]. Knowledge of this function is important for determination of all quantitative corrections except for fluorescence by the continuum [55].

Philibert [3] derived the $\phi(\rho z)$ curves from a theoretical treatment by considering excitation in a thin layer $d(\rho z)$ in depth ρz in a complex target. The following is his derivation of an expression for $F(\chi)$.

Consider an electron passing through the layer dz on a path making an angle ϕ_i with the normal to the sample surface. The number of ionizations of A atoms, n_i in the shell which results in emission of the analytical line caused by this electron is given by

$$n_i = \rho C_A \frac{N}{A_A} Q_A \frac{dz}{\cos \phi_i} \qquad (1\text{-}8)$$

where N is Avagadros number, A_A is the atomic weight of A, Q_A is the ionization cross-section for the shell of element A which results in emission of the analytical line.

The total number of ionizations per unit area of dz is then given by the sum of equation (1-8) for all electrons

crossing the layer dz. If the total number of electrons crossing the layer is r $n_o(z)$, then

$$\sum_{i=1}^{r\, n_o(z)} n_i = \rho\, C_A \frac{N}{A_A} Q_A \sum_{i=1}^{r\, n_o(z)} \frac{dz}{\cos \phi_i} \qquad (1\text{-}9)$$

To obtain the intensity of the analytical line dI_A, equation (1-9) should be multiplied by the product of the fluorescence yield ω_A and the probability of emission of the specific spectral line P_{iA}. Therefore,

$$dI_A = \omega_A P_{iA} \rho\, C_A \frac{N}{A_A} Q_A \sum_{i=1}^{r\, n_o(z)} \frac{dz}{\cos \phi_i} \qquad (1\text{-}10)$$

Neglecting $\omega_A P_{iA}$ as has been done in reference [3] does not introduce an error in Philibert's expression since the $F(\chi)$ curves are calculated on a relative basis and any constant factors are cancelled.

To evaluate the sum in equation (1-10) let n_o be the number of electrons striking a unit area of the target and $n_o(z)$ be the number at a depth ρz. This accounts only for the electrons passing downwards through the layer. As a result of backscattering, the total number of electrons crossing the layer can be written $n_o(z)\, r(\rho z)$, where $r(\rho z)$ is a fraction dependent on depth in the sample. The angular dependence of the electron paths on $r(\rho z)$ is introduced by defining

$$R(\rho z) = \frac{1}{n_o(z)} \sum_{i=1}^{r\, n_o(z)} \frac{1}{\cos \phi_i} . \qquad (1\text{-}11)$$

$R(\rho z) \times d(\rho z)$ then is the mean electron path through the layer per incident (downward) electron.

Substituting in (1-10) yields

$$dI_A = \omega_A P_{iA} C_A \frac{N}{A_A} Q_A n_o(z) R(\rho z) d(\rho z). \quad (1\text{-}12)$$

$R(\rho z)$ is assumed to follow a simple exponential low from R_o at the surface of the sample to R_∞ at a depth where the electrons are completely diffused. Therefore

$$R(\rho z) = R_\infty - (R_\infty - R_o) \exp(-k\rho z). \quad (1\text{-}13)$$

Some additional assumptions are needed to compare the equation (1-12) with the experimental curves of Castaing and Descamps [2]. First the number of electrons $n_o(z)$ is assumed to vary with depth according to Lenard's law

$$n_o(z) = n_o \exp(-\sigma \rho z), \quad (1\text{-}14)$$

where the Lenard coefficient σ depends only on the accelerating voltage E_o of the electron beam. Secondly, using the same approximation as Castaing [20], the ionization cross section Q_A is assumed to be constant for a given shell of a given atomic number element. Therefore, Q_A is independent of depth. Using these two assumptions and substituting for $R(\rho z)$ in (1-12),

$$dI_A = R_o R_\infty \omega_A P_{iA} C_A \frac{N}{A_A} Q_A \{\exp(-\sigma \rho z) - (1 - \frac{R_o}{R_\infty}) \exp[-(\sigma + k)\rho z]\} \quad (1\text{-}15)$$

Because the experimental $\phi(\rho z)$ functions are measured on

a relative basis to a layer of the pure element isolated in space, R_o, ω_A, P_{iA}, and C_A disappear in the expression for $\phi_A(\rho z)$ and the expression of Philibert is obtained

$$\phi_A(\rho z) = R_\infty \frac{N}{A_A} Q_A \{\exp(-\sigma \rho z) - (1 - \frac{R_o}{R_\infty}) \exp[-(\sigma + k)\rho z]\} \quad (1\text{-}16)$$

The parameter k can be calculated from Bothe's scattering law [21]. According to this law the standard deviation of the angle of the electron path from the normal is given by

$$\psi \approx \frac{400}{E_o} (\frac{Z_A}{A_A} \rho z)^{1/2} \quad (1\text{-}17)$$

where $\psi = \frac{\pi}{4}$, at depth z_m the electrons are considered fully scattered so that

$$\rho z_m \approx 4 \times 10^{-6} \frac{A_A}{Z_A^2} E_o^2 \quad (1\text{-}18)$$

Assuming that at this depth z_m, $R(\rho z)$ is within 10% of R_∞, i.e., $\exp(-k \rho z_m) = 0.1$, then

$$k \approx \frac{1}{0.43 \rho z_m} = 0.58 \times 10^6 \frac{Z_A}{A_Z} \frac{1}{E_o^2} \quad (1\text{-}19)$$

Good agreement with Castaing and Descamp's experimental curve for copper, aluminum, and gold was obtained using the k of (1-19).

By taking the Laplace transform of equation (1-16) and dropping the constant terms, the expression for $F(\chi)$ is obtained, i.e.,

$$F(\chi) = \frac{1}{1 + h(1 + \frac{\chi}{\sigma})} \left[\frac{1}{1 + \frac{\chi}{\sigma}} + h \frac{R_o}{R_\infty}\right] \qquad (1\text{-}20)$$

where $h = \sigma/k$.

Because R_o and R_∞ are not easily obtained, a simplified form of this equation in which the final term is dropped is used for the absorption correction. This equation is

$$F(\chi) = \frac{1}{(1 + \frac{\chi}{\sigma})\ [1 + h(1 + \frac{\chi}{\sigma})]}. \qquad (1\text{-}21)$$

The parameter h is given by

$$h = 1.72 \times 10^{-6} \frac{A}{Z} \sigma E_o^2 = \text{constant} \frac{A}{Z^2} \qquad (1\text{-}22)$$

Since for accelerating voltages greater than 30 k.v. the product of σE_o^2 is a constant, h depends only on the atomic number and atomic weight of the target. Electron scattering by the target material is corrected for by h which varies as the target material varies. Mean values of $\bar{A}$ and $\bar{Z}$ should be used in calculating h in the sample, using the equations

$$\bar{Z} = \sum_i N_i Z_i \text{ and } \bar{A} = \sum_i N_i A_i \qquad (1\text{-}23)$$

where N_i are the atomic concentrations.

The simplification of equation (1-21) makes fitting of the $\phi(\rho z)$ curves impossible using the values for h and σ as defined above. However, the $F(\chi)$ curves can still be fitted accurately by modifying the values of h and σ. Values of σ are given by Philibert [3] using for h the expression

$$h = 1.2 \frac{A}{Z^2} \qquad (1\text{-}24)$$

so that agreement between the experimental $F(\chi)$ curves and the calculated values is quite good. $F(\chi)$, as defined in (1-21), depends on atomic number, since when, $\chi = 0$, $F(\chi) = 1/(1 + h)$. To remove this dependence on atomic number a new $f(\chi)$ has been defined which is equal to $(1 + h) \times F(\chi)$ [54]. The equation for $f(\chi)$ is now generally referred to as Philibert's expression.

The $f(\chi)$ curves can be measured directly by measuring the intensity from a pure sample as a function of take-off angle ψ and hence as a function of χ since $\chi = \mu \csc \psi$. As a result of the work of Green [19] on measurement of $f(\chi)$ curves, Duncumb and Shield [6] have proposed modification of Philibert's expression for $f(\chi)$ by substitution of the expression

$$\sigma = \frac{2.39 \times 10^5}{E_o^{1.5} - E_c^{1.5}} \qquad (1\text{-}25)$$

where E_c is the critical excitation energy. E_o and E_c are in kilovolts. Better agreement is found between measured and calculated curves at low electron voltages when this expression is used. Heinrich proposed a different constant [50] for σ

$$\sigma = 4.5 \times 10^5/(E_o^{1.65} - E_c^{1.65})$$

based on analysis of $f(\chi)$ curves then available.

Measurements of x-ray intensity versus depth of emission, $\phi(\rho z)$ can be used to accurately calculate quantitative corrections. However direct measurements of $\phi(\rho z)$ are quite tedious. Castaing and Descamps [2], and Vignes and Dez [35] measured a number of $\phi(\rho z)$ curves to determine the absorption correction. This method was used by J.D. Brown [10] for estimation of characteristic fluorescence effects and by J.D. Brown and L. Parobek [56] for determination of the atomic number effect. It is theoretically possible to obtain $\phi(\rho z)$ curves from the more easily measured $f(\chi)$ curves by an inverse transformation. Such a method has been described by Kilpatrick and Hare [22].

The $f(\chi)$ curves and $\phi(\rho z)$ curves have been calculated using theoreticaly models. Using quite different approximations to the interactions of electrons with matter, Archard [23] and D.B. Brown [46] have obtained good agreement with

the experimental $f(\chi)$ curves. However, while Brown's model also accurately predicts $\phi(\rho z)$ curves, Archard obtained a very different distribution of intensity with depth than is actually observed. This points to the fact that the shape of the $f(\chi)$ curves is rather insensitive to the $\phi(\rho z)$ distribution, and hence suggests that the inverse transformation method would be subject to a large error. Also, very good results for $\phi(\rho z)$ curves were obtained by Monte Carlo calculations. All three methods are described in Chapter III.

CHAPTER II

The Atomic Number Effect

The atomic number effect has been defined as a difference in the number of x-rays produced per electron in matrices of different atomic number. It results from different behaviour of the electrons in materials of different atomic number. When an electron beam is incident on an alloy of low mean atomic number $\bar{Z}$ a smaller fraction of electrons are back-scattered than from a standard of high atomic number. This leads to a relative enhancement of the x-ray intensity from the alloy. On the other hand, the electrons lose energy more rapidly in the alloy (per unit mass thickness), have less opportunity to produce ionizations, and thus generate a relatively reduced x-ray intensity. The balance of these two factors is such, that, in general, a low $\bar{Z}$ alloy referred to a high Z standard will have an intensity ratio of x-rays generated in the sample which is less than the mass concentration of the analyzed element.

For simplicity in the discussions which follow, let us consider the analysis of the element A in a binary sample AB. The analysis is done with reference to a pure standard, A, and the data was obtained as the ratio, I_{AB}/I_A of the intensity of the characteristic x-ray emission from the sample to that from the pure standard, A. More complex

situations involving multicomponent systems, which arise in practice can generally be dealt with by a simple extension of the binary method.

Proposed Methods of Correction

The objective of a correction procedure is to estimate the factor relating the intensity ratio K_A to concentration, C_A, in the expression introduced in Chapter I.

$$K_A = C_A \frac{\int_0^\infty \phi_{AB}(\rho z) \exp(-\chi_{AB} \rho z)\, d(\rho z)}{\int_0^\infty \phi_A(\rho z) \exp(-\chi_A \rho z)\, d(\rho z)} \qquad (2\text{-}1)$$

This expression is exact in the absence of fluorescence effects and includes the two main corrections, atomic number and absorption, since each $d(\rho z)$ element of generation (through ϕ) is linked to the appropriate absorption path (through χ).

Many methods have been proposed to evaluate the correction factor linking measured intensities to concentration in equation (2-1). Poole [32] proposed that the methods can be divided into three main groups:

I. The estimation of the function $\phi(\rho z)$ and the associated absorption effect either theoretically or empirically. This method has been extensively used and can be regarded as having three sub-methods; I_a, I_b, and I_c covering calculations

using models of individual electron behavior by means of scattering parameters, etc., and empirical approaches which combine the whole correction into a single parameter;

II. The approach whereby the x-ray intensity and distribution is considered as dependent on electron backscatter and retardation terms and on the ionization cross section Q(E). The absorption correction is evaluated separately.

III. Measurement of the function $\phi(\rho z)$ for alloys and standards of interest so that equation (2-1) could be evaluated separately.

Method I - Estimation of $\phi(\rho z)$ from a consideration of individual electron behavior can be carried out in various ways. For example, a large number of electrons can be followed through a large number of interactions with the target material by a Monte Carlo type calculation, with or without simplifications to make the calculation more manageable. An example of the latter approach is that of Archard and Mulvey (1962) [12], and R.C. Wolfe and V.G. Macres [24] in which a relatively simple model of the behavior of a selection of individual electrons was used. The model is one which has already been shown, Archard (1961) [23], to represent the backscatter process adquately. A simple extension enabled x-ray yield and absorption effects of

equation (2-1) to be calculated for selected metal and alloy targets under various excitation conditions from which curves were obtained of the variation with composition of both the atomic number and absorption effects in a few alloy systems. Strictly, the correction factor curves can only be used for those systems to which they refer and the method cannot be generally used. A real limitation on these methods is the difficulty in calculation and the expense of extensive computer time.

Method I$_b$ - This method evolved from consideration of the $\phi(\rho z)$ function. However, the curious point emerges that all the workable procedures involve the introduction of factors into the absorption terms in order to correct for the atomic number effect, even though the latter is really one of generation, i.e., the correction for $\phi(\rho z)$ shape is being modified in an attempt to correct for area differences.

Castaing (1951) in his thesis [1] introduced an empirical α term describing the properties of each element such that the generated intensity ratio, K' is given by

$$K' = C_A \alpha_A / (C_A \alpha_A + C_B \alpha_B). \qquad (2\text{-}2)$$

This expression involves the assumption, among others, that

$$\int_0^\infty \phi_A(\rho z)\, d(\rho z) \Big/ \int_0^\infty \phi_B(\rho z)\, d(\rho z) = (\alpha_B/\alpha_A) \qquad (2\text{-}3)$$

ϕ_A, ϕ_B here describing the characteristic radiation of A in pure A, and the same radiation in effectively pure B, respectively.

In his later publications, Castaing (1960) [11] suggests that α is the product of two Z-dependent factors: one factor describing the effect of backscattering and the second factor describing the effect of deceleration[1] taken at that time as Z/A following Webster (1928) [25].

Absorption terms, $F(\chi)$ or $f(\chi)$, according to assumptions made[2] can then be introduced such that the emitted intensity ratio, K, is related to the generated intensity by:

$$K = K' [F(\chi)_{AB}/F(\chi)_A]. \qquad (2\text{-}4)$$

Philibert (1961) [26], as was mentioned in Chapter I, derived an expression for $F(\chi)$ from an electron distribution model which enabled the x-ray distribution function to be estimated in various target materials. His expression

$$1/F(\chi) = (1 + \chi/\sigma) [1 + h (1 + \chi/\acute{\sigma})] \qquad (2\text{-}5)$$

introduced the parameter h (= $1.2\ A/Z^2$) which enabled the function to be calculated for any pure metal target (σ is a Lenard coefficient dependent on incident voltage); by introducing a factor h, calculated from the mean $\overline{A/Z^2}$

---

[1] These two factors in recent work are described by R and S, respectively.

[2] $F(\chi)$ and $f(\chi)$ are related by the expression $f(\chi) = F(\chi)/F(0)$ where $F(0)$ refers to $F(\chi)$ when $\chi = 0$.

value for the alloy, the absorption function for the alloy target could also be calculated. The parameter h takes into account the atomic number part of the absorption correction but does not, however, constitute a correction for the atomic number effect as such, although at the time this was not universally appreciated.

About the same time, Theisen (1961) [14] and Tong (1961) [27] produced an expression for $F(\chi)$, exactly similar to those of Philibert, which was claimed to perform the whole of the necessary correction from intensity ratio to concentration when used in the equation

$$K = C[F(\chi)_{AB}/F(\chi)_{A}]. \qquad (2\text{-}6)$$

The parameter h (called ξ) in Theisen's expression was evaluated from

$$h = 3.5\ A/Z^2 \qquad (2\text{-}7)$$

In his book, Birks (1963) [9] put forward a simplified method of absorption correction into which he introduced a factor p, dependent on Z, which was used to adjust the value of χ before reading $F(\chi)$ from the tables provided. The $F(\chi)$ values were then used in a simple expression identical to equation (2-6). This procedure was "... to make a correction for the variation of $\phi(\rho z)$", and was claimed to perform the atomic number correction.

Theisen in his book (1965) [28] modified his formula of 1961 to

$$K = C(R_{AB}/R_A)\ [f(\chi)_{AB}/f(\chi)_A] \qquad (2\text{-}8)$$

where R is an effective current factor {after Thomas (1963 [16]} to allow for backscatter loss and $f(\chi)$ is used instead of $F(\chi)$, and is calculated from

$$1/f(\chi) = (1 + \chi/\sigma_E)\ [1 + (\frac{h}{1+h})\ \chi/\sigma_E] \qquad (2\text{-}9)$$

where σ_E is a modified Lenard coefficient taking into account overvoltage

$$\sigma_E = [8.9 \times 10^5/(E_o - E_c)^2] \qquad (2\text{-}10)$$

and h now combined atomic number and voltage terms in the expression

$$h = 1.72 \times 10^{-6}\ E_o^2\ A/Z^2.$$

Method I_c - Ziebold and Ogilvie (1964) [13] proposed a method by which both the atomic number and the absorption effects were combined into a single parameter, α. This was employed in the relation

$$(1 - k)k = \alpha(1 - C)C. \qquad (2\text{-}12)$$

The derivation of the expression by which α may be readily calculated has its origins in Method II, i.e., it takes into consideration backscatter and retardation terms - but since the atomic number and absorption effect are combined into a single parameter discussion in this section is appropriate. The expression for α is

$$\alpha = 0.95 \left(\frac{\sigma + \chi_B}{\sigma + \chi_A}\right)\left(\frac{Z_A}{Z_B}\right) 0.28. \qquad (2\text{-}13)$$

where σ is an original Lenard coefficient.

A second method relying on a single parameter to combine both major corrections is that of Traill and Lachance (1965) [47,48] who discuss the general area of spectrochemical analysis of multicomponent systems; they demonstrate that the expression

$$K = C_A/(1 + C_B\ \alpha_{AB}) \qquad (2\text{-}14)$$

adequately represents observed intensity ratios in selected analytical examples when α_{AB} is chosen to suit the particular system investigated. The evaluation of α can either be by calibration or by a combination of absorption, atomic number and fluorescence corrections calculated by some such approach as those in Method II; to this extent the method would not seem to have great advantage except, perhaps, for work involving a calibration procedure.

Both these methods of I_c, in fact, come from similar work done in x-ray spectrometry for correction of matrix effects. The basic assumption which is made in such procedures is that the effect of an atom of one element on the intensity emitted by a second element is the same regardless of concentration and the presence of other elements in the sample.

Method II_a - This method involves approximating the initial intensity ratio by an expression involving atomic

number and absorption terms separately, viz:

$$K_A = C_A \frac{R_{AB} \int_{E_C}^{E_O} Q_{AB}(E)/S_{AB}(E)\,dE}{R_A \int_{E_C}^{E_O} Q_A(E)/S_A(E)\,dE} \times \frac{(\text{Absorption Factor})_{AB}}{(\text{Absorption Factor})_A} \qquad (2\text{-}15)$$

Here $\underline{R}$ is the effective current factor, already introduced, which takes account of the loss of ionization due to back-scatter. $Q(E)$ is the ionization cross section for the radiation concerned and $S(E)$ is the stopping power of the target for electrons of energy E, defined as

$$-\frac{1}{S} = \frac{dE}{dx}.$$

Approximations and empirical factors are then introduced to enable the atomic number part of expression (2-15) to be evaluated.

In their first method, Poole and Thomas (1962) [17] followed the lead offered by Castaing's early work, and by assuming that S was constant, and that

$$\int_{E_C}^{E_O} Q_{AB}(E) \Big/ \int_{E_C}^{E_O} Q_A(E) = 1. \qquad (2\text{-}16)$$

They reduced (2-15) to the form

$$K_A = C_A \frac{R_{AB}}{S_{AB}} \frac{S_A}{R_A} \frac{(\text{Absorption Function})_{AB}}{(\text{Absorption Function})_A} \qquad (2\text{-}17)$$

or

$$K_A = \frac{C_A \alpha_A}{C_A \alpha_A + C_B \alpha_B} \frac{F(\chi)_{AB}}{F(\chi)_A} \qquad (2\text{-}18)$$

which is identical to the combination of Castaing's equation (2-2) and 2-4), and which assumes that

$$(S_{AB}/R_{AB}) = \alpha_{AB} \equiv C_A \alpha_A + C_B \alpha_B \qquad (2\text{-}19)$$

with

$$S_A/R_A = \alpha_A \text{ and } S_B/R_B = \alpha_B \qquad (2\text{-}20)$$

S was evaluated from Nelm's tabulation [29] taken at 30 keV, and R was taken from an empirical curve of the variation with Z which had been estimated from the results of a few analyses. At this stage the proposed correction for atomic number effect takes no account of excitation conditions.

This method was quite promising but was soon revised by Thomas (1963) [16] to take into account the excitation conditions. In this version, equation (2-17) was still used but R was taken from curves of R versus Z and overvoltage (E_o/E_c) which had been estimated by a rough approximation from published backscatter data. S was still obtained from Nelm's tables but was taken at $E = (E_o + E_c)/2$.

The procedure also involved a special way of attempting to allow for the atomic number part of the absorption correction; namely, the use of the same value of h ($=h_A$) in Philibert's expression for $F(\chi)$ for both alloy and standard, coupled with a modification of χ_{AB} to the form

$$\chi'_{AB} = \frac{\chi_{AB}}{C_A - C_B\ (\alpha_B/\alpha_A)}. \qquad (2\text{-}21)$$

This procedure has not been universally accepted as reasonable.

Working from the voltage independent atomic number correction of the type proposed by Poole and Thomas, and from Philibert's absorption correction procedure, Belk (1964) [18] produced a gross simplification enabling the complete correction to be reduced to

$$C_A = K_A \left[1 + \frac{\bar{Z}_A - Z_{AB}}{100}\right] \left[1 + \frac{\mu_{AB} - \mu_A}{P + \mu_A}\right] \qquad (2\text{-}22)$$

where

$$P = \sigma . \sin\theta\ [(1 + h)/(1 + 2h)] \qquad (2\text{-}23)$$

and if the atomic number Z of any component exceeds 40, it should be represented by a $Z' = 40 + 0.3\ (Z - 40)$. The method will not work well when the absorption correction is large and Belk has set limits outside which errors greater than 2% can be expected. Despite its extreme

simplicity, the method works very well and compares favorably with the more complicated methods.

Smith (1965) [30] has also evolved a method for evaluating the terms S/R in the correction equation (2-17); he has utilized the more rigorously determined R curves of Green (1963) [31] and an empirical expression for S (based on one first proposed by Long); namely

$$S = [4.7 + 0.9 \ln (E_o - E_c) - \ln < Z >] < \frac{Z}{A} > \qquad (2\text{-}24).$$

where < > denotes a mean value appropriate to alloy or standard. These terms are put forward for use with a set of mass absorption coefficients which have been specially derived to fit a large number of microanalysis results on mineralogical samples. The tabulation of coefficients are not extensive enough to enable Smith's method to be applied generally [32].

Method II_b - A more rigorous approach has been adopted by Duncumb [49] who has carried through accurate evaluations of the expression $\int Q(E)/S(E) \cdot dE$, and of the backscatter loss. This means he has been able to estimate the errors involved in approximations and simplifications which have been proposed to enable the correction to be simply carried out. For example, he has shown that the assumption of S constant, which is implicit in all the II_a methods, is one which, in general, introduces only a small error. As well as

looking into the finer details, this work has also produced a readily used method - Duncumb (1967) [44]. In this, the familiar S and R terms are employed in an equation identical to (2-17) and S is evaluated from the expression

$$S = \text{const.}\ (\overline{Z/A})\ (1/\overline{E})\ \ln\ (1.166\ \overline{E}/J) \qquad (2\text{-}25)$$

where J is the mean ionization potential for the target material and is evaluated from an empirical relation

$$J/Z = 15.05\ [1 - e^{-0.072Z}] + (42/Z^{Z/10}) - (Z/400) \qquad (2\text{-}26)$$

Equation (2-26) was evolved to give values of J which resulted in the best possible fit between corrected analytical results and known concentration for selected alloys - i.e., microanalytical results have been used to determine the apparent variation of the physical parameter, J. The absorption correction is carried out using Philibert's $f(\chi)$ formula as modified by Duncumb to take account of overvoltage [6]. Poole [32] has collected experimental x-ray data for 229 standard samples of well-known composition. Since in this thesis emphasis is on low electron energies, just 24 samples were selected for comparison with the available correction methods. Compositions were calculated from measured x-ray data on the basis of these methods to compare with the known compositions of the standard samples. The results for the 24 selected samples are tabulated in Table 1.

As can be seen from Table 1 none of the selected

Table 1

Errors Resulting from the Application of the Methods of Ziebold and Ogilbie, Belk, Thomas, Duncumb and Smith.*

System A-B	Radiation	Eo[keV]	True C_A	K_A	Percent Relative Errors				
					Z & O	Belk	Thomas	Duncumb	Smith
U Al_2	U-Mα	11	0.815	0.728	-5.3	-2.9	+1.0	+3.8	-5.6
Ni-Al	Ni-Kα	10	0.421	0.360	-5.4	-6.8	-1.4	-0.4	+0.2
Ni-Al	Ni-Kα	10	0.592	0.525	-4.5	-5.5	-2.7	-0.6	-0.9
Fe-Al	Fe-Kα	10	0.408	0.360	-3.1	-4.2	-2.0	+2.5	+0.5
Ti-Al	Ti-Kα	10	0.372	0.320	-5.4	-5.0	-11.3	-0.6	-2.2
Fe_2O_3	Fe-Kα	12	0.697	0.642	+0.5	-2.9	-0.9	+0.5	-1.7
Fe_2O_3	Fe-Kα	15	0.697	0.647	+1.0	-2.3	-1.1	+0.2	-2.0
Cu-Al	Cu-Kα	12.2	0.041	0.033	-5.0	+5.6	+0.5	+6.4	+6.8
Al_3Ni	Al-Kα	10	0.579	0.385	-6.3	+2.2	+7.5	+10.7	+4.1
Al_3Ni_2	Al-Kα	10	0.408	0.247	-6.1	+5.2	+15.1	+15.6	+7.7
Al_3Fe	Al-Kα	10	0.592	0.446	-3.4	+5.6	+8.4	+11.7	+5.2
Al_3Ti	Al-Kα	10	0.628	0.511	-8.4	-2.1	+2.2	-0.1	-3.9
Al_6Mn	Al-Kα	10	0.747	0.640	-3.3	+2.5	+3.2	+3.4	+0.4
Al_3Fe	Al-Kα	10	0.580	0.459	-7.6	+1.6	+3.9	+4.3	0.0
Al_9Co_2	Al-Kα	10	0.673	0.541	-2.8	+5.9	+7.2	+7.6	-3.4
Al_3Ni	Al-Kα	10	0.580	0.415	-5.9	+5.1	+8.4	+9.2	+4.4
Al_3Mg_2	Al-Kα	10	0.640	0.460	+1.6	-7.1	+6.8	+11.0	+7.9
Al_2Cu	Al-Kα	10	0.460	0.310	0.0	+10.5	+17.3	+16.0	+8.6
UC_2	U-Mβ	10	0.908	0.855	+1.0	-1.6	+1.9	+2.0	-3.7
UN	U-Mβ	10	0.944	0.910	+0.4	-1.0	+1.1	+1.2	-2.5
U_3Si	U-Mβ	10	0.962	0.939	-0.4	-0.5	+0.8	+0.9	-1.4
UP	U-Mβ	10	0.885	0.822	-1.6	-1.7	+2.4	+2.4	-3.3
US	U-Mβ	10	0.881	0.814	-2.1	-1.9	+2.1	+2.5	-3.3
U_6Fe	U-Mβ	10	0.962	0.945	-0.7	-0.7	+0.4	+0.4	-1.1

* Calculated compositions based on experimental data collected by Poole [32]

methods is totally satisfactory. The relative errors were calculated according to the formula

$$\% \text{ rel. error} = \frac{C_{cal.} - C_{true}}{C_{true}} 100$$

and are as much as + 17% for Thomas method and as much as + 16% for Dumcumb and Reed method in case of Al_2Cu system when Al-Kα line was analyzed. These two methods are considered to be the most successful methods for calculation of the atomic number effect. Thus the atomic number correction or absorption correction used in the methods were overestimated.

Method III - This method relies on the exact determination of the $\phi(\rho z)$ curves. Two methods were developed for the measurement of the $\phi(\rho z)$ curves, the sandwich sample technique [2] and wedge-shaped sample technique [57].

A cross-section of a wedge-shaped specimen is shown in Fig. 2. The two elements A and B have to satisfy the following conditions:

1. The elements must have almost the same atomic number.

2. The atomic number of element A must be higher than the atomic number of element B. The second condition is important in order to avoid fluorescence effects. The x-ray signal is taken only from the element A.

When the electron beam is moved from B (left hand side) towards the A-wedge the characteristic x-ray signal in A

is generated after the electron beam has passed the tip of the wedge. The intensity $I(\rho z)$ of this signal is measured as a function of the distance from the tip of the wedge. If an angle of the wedge and a density ρ of material A is known this distance can be directly converted into ρz values. The increase of $I(\rho z)$ with increasing ρz provides the experimental information from which the depth distribution $\phi(\rho z)$ can be deduced.

$$\phi(\rho z) = \text{constant} \frac{d}{d\rho z} I'(\rho z)$$

where $I'(\rho z)$ represents the primary x-ray intensity generated in the wedge A. The measured intensity $I(\rho z)$ and the intensity $I'(\rho z)$ are related to each other by

$$dI'(\rho z) = dI(\rho z) \exp(-\chi \rho z).$$

It follows that

$$I(\rho z) = \int_0^{\rho z} \frac{dI'(\rho z)}{d(\rho z)} \exp(\chi \rho z)\, d(\rho z).$$

This technique can be useful for determining the absorption correction but cannot be used for determining the atomic number correction.

The second method for determining the $\phi(\rho z)$ curves directly is the sandwich sample technique first described by Castaing and Descamps [2]. The cross-section of the sandwich sample is shown in Fig. 1. The sandwich samples can be prepared as follows. On a solid block of one pure element, A, a thin layer of a second element, B, the

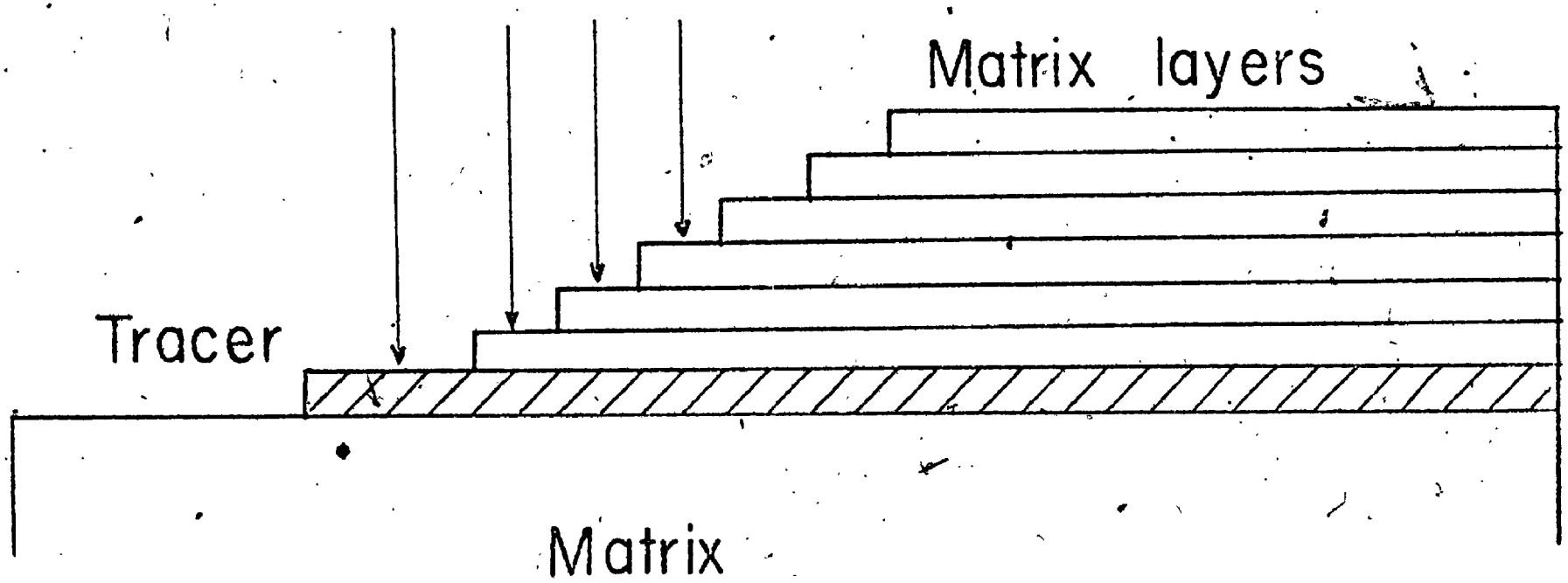

Figure 1. Sandwich Sample Usually Used to Determine $\phi(\rho z)$ Curves

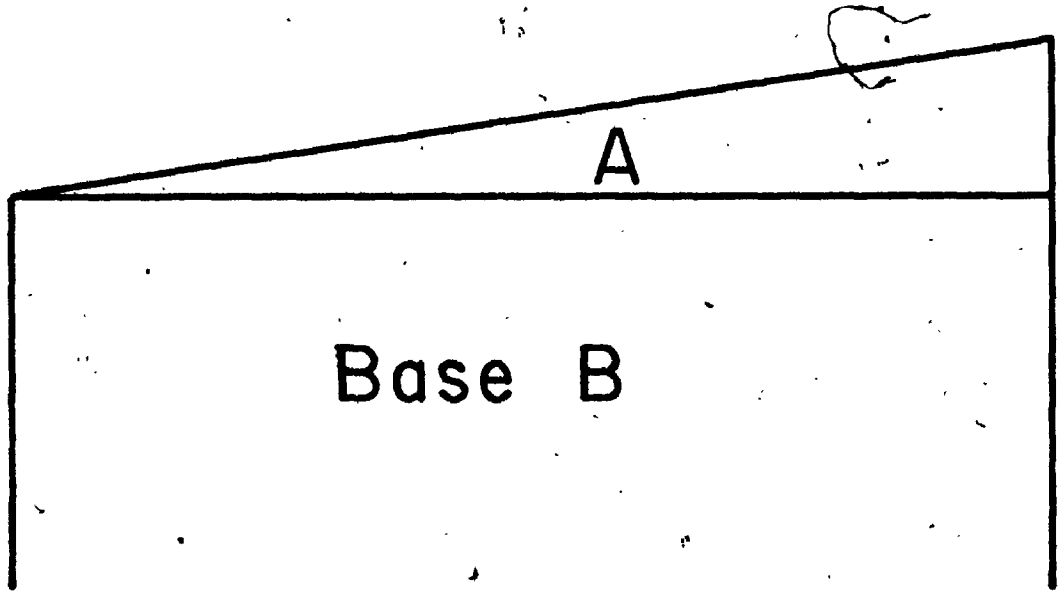

Figure 2. The cross section of the Wedge-Shaped Specimen

tracer is plated. This in turn is covered by successively thicker layers of the element A. Intensity measurements of the characteristic x-rays from the layer of element B on each step gives the $\phi(\rho z)$ curve after corrections have been made for absorption in the sample and secondary fluorescence by the continuum. Since the geometry is known the correction for absorption is straight forward.

If layers of identical thickness of a single tracer element are deposited within sandwich samples having a different atomic number of the matrix element, then differences in the measured depth distribution will be due to the difference in back-scattering and stopping power of the matrix elements. These differences are just those ascribed to the atomic number effect. The distributions of x-ray production obtained are for a small concentration of the tracer element in the matrix elements. Proper selection of trace element and matrix elements eliminate contributions due to the fluorescence by characteristic lines and the depth distribution curves obtained by this technique corrected for fluorescence by the continuum should characterize the atomic number effect.

The advantage of the sandwich sample method against the wedge-shaped sample method is that the atomic numbers of the tracer and matrix do not have to be almost the same; an essential condition in the wedge-shaped sample method.

Hence the atomic number and the absorption correction can be studied simultaneously and is the basis of the measurements described in this thesis.

CHAPTER III

Theoretical Calculations of Depth Distribution Curves

Three theoretical approaches have been used which can yield a calculated distribution of x-ray production as a function of depth in the sample; the Diffusion Model, the Transport Equation, and Monte Carlo Technique. The following briefly outlines these methods.

Diffusion Model

When a sample target is exposed to an electron beam, the incident electrons undergo a series of elastic and inelastic collisions with the target atoms. Inelastic collisions result in a deceleration, loss of energy of the incident electrons, and a subsequent emission of characteristic x-rays by excited target atoms. During the deceleration process an electron may change direction many times and may escape from the target before its energy is expended, thus contributing to backscatter losses.

In order to evaluate the electron deceleration process, it is necessary to obtain an expression for the electron path during which primary emission occurs. Bethe, et al [38] approached the problem by assuming that electrons travel straight into the target to a given depth after which they diffuse randomly in all directions. This approach, often referred to as the electron diffusion theory, assumes

that elastic deflections which an electron may undergo before reaching this depth of complete diffusion are negligible. Archard [25] has pointed out that for atomic numbers greater than 6, the contribution from elastic scattering is small. In such cases, therefore, the fraction of electrons back-scattered may be calculated using the Bethe approach.

The loss of energy by electrons in passing through a solid target of a pure element has been expressed by Archard and Mulvey [40] using Bethe's deceleration law

$$\frac{dE}{dx} = -\left(\frac{2\pi\ NZ\ e^4}{E}\right) \ln\left(\frac{2\ E}{J}\right) \qquad (3\text{-}1)$$

where e is an electron charge in electrostatic units; E is energy of electrons; Z is atomic number of target; N is number of atoms per cm^3; J is mean ionization potential of target atoms (J = 11.5 Z E); and x is the path length travelled by electrons in centimeters.

Integration of equation (3-1) gives

$$x = \left(\frac{7.68 \times 10^{12}}{NZ\ e}\right) [E_o^2\ F(E_o) - E^2\ F\ (E)] \qquad (3\text{-}2)$$

where E_o - initial energy, in electron volts

$$F(E) = 1/y\ (1 + 1/y + 2!/y^2 + ...)$$

$$y = 2\ \ln\ (0.174\ E/2e)$$

To determine F(E), the semiconvergent series is taken only as far as its smallest term. By substituting the relation $N = \rho N_A/A$ in equation (3-2), the relation for the electron penetration can be expressed in terms of ρx

$$\rho x = \frac{7.68 \times 10^{12}}{N_A \, Z/A \, e} \left[E_o^2 \, F(E_o) - E^2 F(E)\right] \qquad (3\text{-}3)$$

where ρ is density in gm/cm^3; A is atomic weight of element; and N_A is Avogadro's number.

Worthington and Tomlin [41] have assumed that electrons effectively come to rest when the function $F(E) = 0$, rather than when $E = 0$, since $F(E)$ becomes indeterminate at $E = 0$, and such a condition does not correspond to physical reality. From equation (3-3) the full range of electron penetration, ρx_r, then becomes

$$\rho x_r = \frac{7.68 \times 10^{12} \, E_o^2}{N_A \, Z/A \, e^2} \, F(E_o) \qquad (3\text{-}4)$$

However, in calculating the intensity of characteristic radiation excited in a target, the electron penetration of primary interest is that which occurs between electron energies E_o and E_c, where E_c is the critical excitation energy required to excite characteristic radiation. After the electron energy falls below E_c, it is unable to excite the characteristic radiation and, therefore, is not of interest in the intensity calculations. The range of electron energies, E_o to E_c, over which primary emission occurs is often referred to as the effective range of electrons, and the effective depth of penetration, ρx_r, as determined by equation (3-3), becomes

$$\rho x_r = \frac{7.68 \times 10^{12}}{N_A \, Z/A \, e^2} \left[E_o^2 \, F(E_o) - E_c^2 \, F(E_c)\right] \qquad (3\text{-}5)$$

The effective penetration, ρx_r, may be considerably less than the full penetration of electrons, ρx_r, especially for low electron energies where the ratio E_o/E_c becomes small.

In using the Bethe diffusion theory, the depth of penetration at which complete diffusion occurs must be determined. Bethe, et al [38] define this depth as that at which the average cosine of the angle between the actual direction of motion of an electron and the direction of the primary electron beam becomes 1/e. Under these circumstances, the Bethe deceleration equation may be expressed as

$$\int_{E_d}^{E_o} \frac{Z \ln (0.54\, E^{1/2}\, e^{-1/2}\, Z^{-1/3})}{4 \ln (0.174\, E/Z\, e)} dE = \frac{E}{2e} \qquad (3\text{-}6)$$

where E_d is the electron energy at ρx_d, the depth of complete diffusion.

Calculation of Intensity

In the diffusion model, electrons are assumed to travel in straight lines into the target until reaching the depth of complete diffusion, and thereafter travel with equal probability in all directions. The intensity of characteristic quanta emitted in any electron path increment may be expressed in terms of the ionization cross section. The total intensity I' of characteristic radiation excited in a target of a single element is

$$I' = \Sigma\, N\, Q\, dx \qquad (3\text{-}7)$$

Where N is number of atoms per cubic centimeter, Q is ionization cross section, and dx is increment of path length travelled by an electron. By combining the differential form of equation (3-2) with equation (3-7) the intensity generated in a pure element target becomes

$$I' = \Sigma \int \frac{7.68 \times 10^{12} Q \, d[E^2 e^{-2} F(E)]}{Z} \qquad (3\text{-}8)$$

For the ionization cross section, Q for K radiation, Mott and Massey [41] give an expression

$$Q = \frac{4.56 \times 10^{-14}}{E/E_c} \ln \left[\frac{4 E/E_c}{1.65 + 2.35 \exp (1 - E/E_c)}\right] \qquad (3\text{-}9)$$

Burhop [43] had shown that the Q-E curve for L radiation has the same form as the expression given by Mott and Massey except for the numerical constant. However, in the intensity equations, the absolute value of Q is not required since it cancels when determining intensity ratios.

Transport Equation

The second theoretical model for predicting the distribution of the x-ray production with depth is the transport equation. The problem of electron transport in solids was treated in 1938 by Bethe, Rose and Smith [38]. The principal assumptions in their treatment were:

1. Scattering of incident electrons takes place by a series of two-particle interattions between the electrons and the target atoms.

2. The energy of these electrons is uniquely related to the distance they have traveled within the specimen.

3. The number of electrons scatterd through a large angle is small. With these assumptions we can write

$$\frac{\partial}{\partial s} f(\bar{r}, \bar{u}, s) = -\bar{u} \cdot \bar{\nabla}_r f(\bar{r}, \bar{u}, s) + \frac{1}{\lambda(s)} \nabla_u^2 f(\bar{r}, \bar{u}, s) \qquad (3\text{-}10)$$

where λ is the transport mean free path defined by

$$1/\lambda = \pi N \int \sin \alpha \, d\alpha \, \sigma(\alpha, s) \, (1-\cos \alpha), \qquad (3\text{-}11)$$

$$\bar{\nabla}_r = \frac{\partial}{\partial r} \bar{J}_r$$

and ∇_u^2 is the operator,

$$\frac{1}{\sin \Theta} \frac{\partial}{\partial \Theta} \left(\sin \Theta \frac{\partial}{\partial \Theta}\right) + \frac{1}{\sin^2 \Theta} \frac{\partial^2}{\partial \Phi^2}. \qquad (3\text{-}12)$$

The remainder of the symbols are defined as follows:

$\bar{r}$ is a position vector (the origin is at a point where incident electrons touch the surface of the target),

s is distance along electron path (in cm),

α is the angle between $\bar{u}$ (before scattering) and $\bar{u}'$ (after scattering),

N is the number of scattering centers (atoms) per unit volume,

$\bar{u}$ is a unit direction of motion vector

$\sigma(\alpha, s)$ is the cross section for deflection of electrons which have traveled distance s through angle α (in cm^2/steradian),

θ is the angle between $\bar{u}$ and the inward normal to the specimen surface,

ϕ is the azimuth of $\bar{u}$ with respect to the inward surface normal,

$f(\bar{r}, \bar{u}, s) \sin\theta \, d\theta \, d\phi \, d^3r$ is the number of electrons having traveled distance s lying in space d^3r around $\bar{r}$ and with $\bar{u}$ laying between θ and $\theta + d\theta$, ϕ and $\phi + d\phi$.

This treatment will take into account the variation of electron density only with respect to one of the three spatial directions, i.e., the depth below the surface, x (in cm). This is mathematically equivalent to an assumption that the current density of electrons impinging on the specimen surface is constant over the surface. It is further assumed that the impinging electrons are monoenergetic, that they have normal incidence to the specimen surface, and that the specimen is homogeneous. With these assumptions, the equations simplify

$$\frac{\partial}{\partial s}\left[\sin\theta \, f(x, \theta, s)\right] = -\frac{\partial}{\partial x}\left[\cos\theta \sin\theta \, f(x, \theta, s)\right] + \frac{\partial}{\partial\theta}\left[\left(\sin\theta \frac{\partial}{\partial\theta}\right)\frac{f(x, \theta, s)}{\lambda(s)}\right] \qquad (3\text{-}13)$$

with the boundary conditions

$f(x, \Theta, s) = 0$ at $x = S_R$,

$f(x, \Theta, s) = \delta(x)\ \delta(\Theta)$ at $s = 0$

$f(x, \Theta, s) = 0$ at $x = 0$ for $s > 0$ and $0 \leq \Theta < \pi/2$,

where S_R is the total range of the incident electrons within the specimen, and $\delta(x)$ and $\delta(\Theta)$ are Dirac delta functions. Equation (3-13) can be solved numerically [36, 37]. Knowning $f(x, \Theta, s)$, it is not difficult to calculate the distribution in depth of primary x-ray production given the probabilities for ionization of the relevant atomic shell. The numerical solution also yields very interesting information on the energy distribution and angle of electrons backscattered from the specimen.

After a large number of collisions, the transport equation can be approximated well by a diffusion equation. We define the total electron density at a given position

$$F(x, s) = \int_{-\pi}^{+\pi} f(x, \Theta, s)\ [2\pi \sin \Theta\ d\Theta]$$

and the current density

$$J(x, s) = \int_{-\pi}^{+\pi} [\cos \Theta\ f(x, \Theta, s)]\ [2\pi \sin \Theta\ d\Theta]$$

then when

$$(1/J)\ (\partial J/\partial s) << (1/\lambda)$$

it can be shown [38] that

$$(\partial F/\partial s) = (\lambda/6)\ (\partial^2 F/\partial x^2)$$

where $\lambda/6$ is a diffusion coefficient.

Monte Carlo Method

The Monte Carlo technique [51, 52, 53] has a quite different structure from the Transport Equation Model. It does not deal with a distribution function but rather makes a random sampling of calculated paths of individual electrons. The simulated electron trajectories (Fig. 3) are generated by using random numbers to determine the new direction and energy of an electron after each scattering event by sampling from the appropriate scattering distribution. Random numbers are also used to establish the distance the electron travels between scattering events. The technique, as just sketched, is often prohibitively expensive in computer time, and in order to reduce the required amount of computation it is common to abandon the complete description of particle histories. In this approximation, the availability of analytical solutions for certain aspects of the multiple scattering is utilized. A "condensed" history is sampled by letting the particle carry out a random walk in which each step takes into account the effect of many collisions [39].

For instance, in the treatment of Bishop [58] of our problem the electron trajectory is divided into 25 steps. The electron is assumed to scatter at some random fraction of the step length through an angle selected from a scattering distribution given by Goudsmit-Saunderson multiple scattering theory [59], which represents the angular

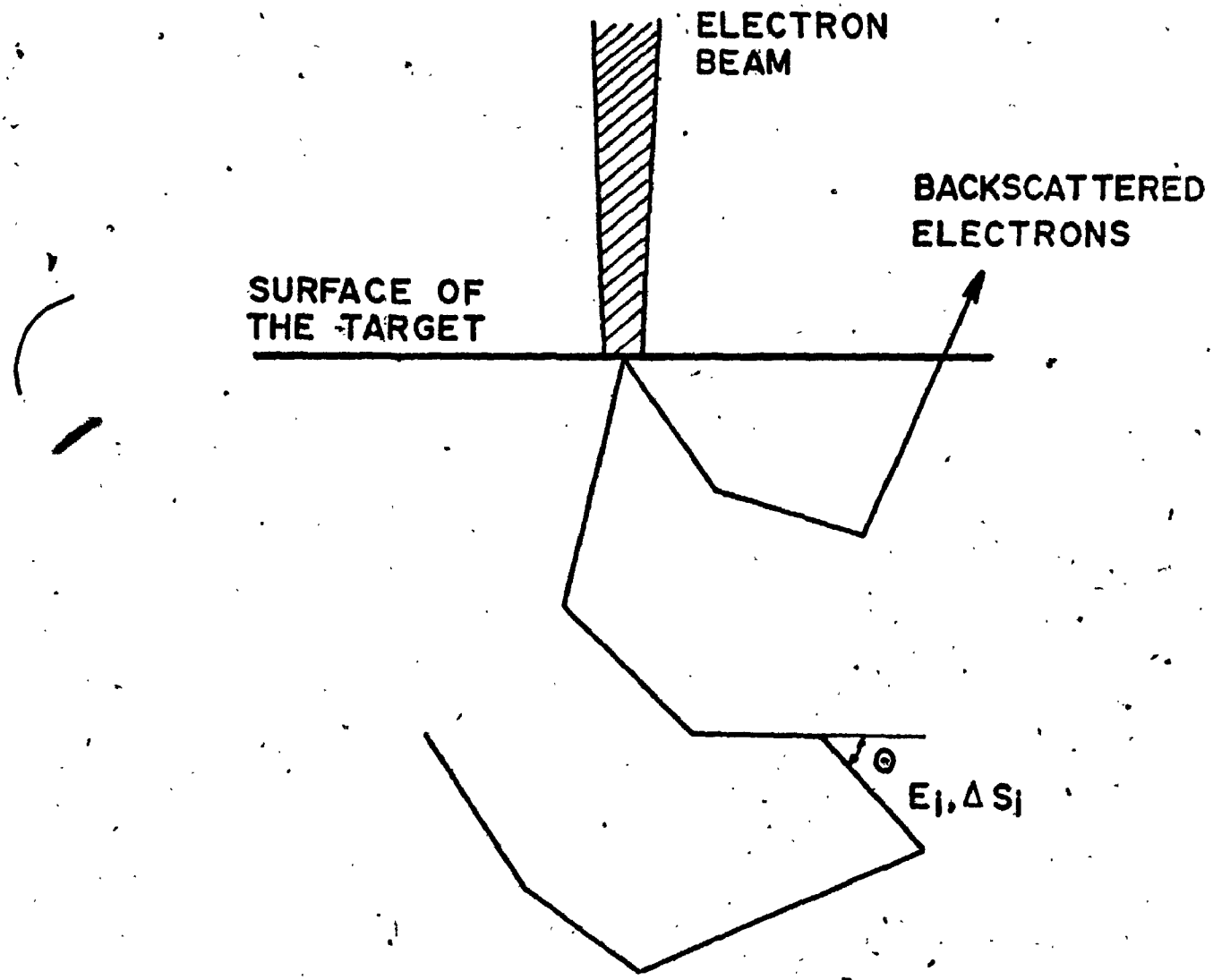

Figure 3. Simplified Model of Electron Trajectory

scattering distributions in terms of Legendre series and has the property of being valid for all scattering angles. Electron trajectories are then generated by random sampling from these data.

A simple screened Rutherford cross section of the differential form

$$\frac{d\sigma}{d\Theta} = 5.2 \times 10^{-21} \frac{Z^2}{E^2} \frac{1}{(1 + 2\alpha - \cos\Theta)^2} \quad [cm^2] \qquad (3\text{-}14)$$

is used to represent the elastic scattering. Here Z is the atomic number of the scattering atom, E is the energy of the incident electron in keV, Θ is the scattering angle and α is a screening factor, an approximate value for which is given by

$$\alpha = 3.4\ Z^{2/3}/E$$

In the energy range of interest (5 - 40 keV) equation (3-14), which is based on the first Born approximation, is not sufficiently accurate to warrant the use of a more complex expression for σ such as that given by Nigam et al [60].

The angular scattering of electrons in elastic events becomes significant for the lighter elements, and therefore equation (3-14) is multiplied by a factor $(Z + 1)/Z$ to make some allowance for this effect.

Although inelastic scattering, like elastic scattering, is a statistical process, the continuous energy-loss approximation is used to simplify the calculation. In this

case the energy loss is represented by the Bethe [40] equation:

$$\frac{dE}{ds} = -7.75 \times 10^4 \frac{\rho}{EZ} \ln (1.166 \frac{E}{J}) \quad [\text{keV cm}^{-1}] \qquad (3\text{-}15)$$

where s is the distance travelled along its trajectory by an electron, ρ is the density of the target, Z its atomic number and J is the mean ionization potential of the target atoms.

Knowing the number of electrons crossing the layer dx in the depth x and their energy, the x-ray intensity generated by these electrons in the layer dx can be calculated. If we, for example, denote by N_K the number of Kα quanta and by n_K the total number of ionizations of the K-shell, then

$$N_K = W\, n_K \qquad (3\text{-}16)$$

where W is the fluorescence yield showing the decrease of the number of Kα quanta due to the Auger effect and is a function of the atomic number.

The number ionizations during the electron travel of length ds becomes

$$dn_K = (N_A\, \rho/A)\, Q_K(E)\, ds$$

where $Q_K(E)$ is the ionization cross-section, N_A is the Avogadro's number and A is the atomic weight. The total number of ionizations per electron is given by

$$n_K = \int_{(s)} \frac{dn_K}{ds}\, ds = \int_{(s)} \frac{N_A\, \rho}{A} Q_K(E)\, ds$$

where s is the path length of the electron traveled in

the layer dx. Then the total x-ray intensity generated in the layer dx is equal

$$I_K = \sum_{K=1}^{n} n_K$$

where n is total number of electrons crossing the layer dx whose energies are higher than the critical energy.,

Shinoda, Murata and Shimizu [53] also used the Monte Carlo calculations to predict the $\phi(\rho z)$ curves. They used a similar approach to the problem as Bishop, but they used different step length and different formulae for calculating α, the screening factor,

$$\alpha = \frac{1}{4} (1.12\, h\lambda/\rho)^2,$$

with

$$\lambda = Z^{1/3}/0.885\, a_o$$

where h is the reduced Plank constant and a_o is the Bohr hydrogen radius.

Comment on Theoretical Models

The $\phi(\rho z)$ curves calculated according to the above described theoretical models usually do not agree well with the experimentally measured $\phi(\rho z)$ curves. This disagreement is especially apparent for diffusion model and for electron energies approaching the critical energy. One source of disagreement which is common for all theoretical models lies in the fact that the calculated intensities represent primary radiation and do not include secondary

radiation excited by the continuum as the experimental curves do. The second source of disagreement is the diffusion model itself. This model is too simple to describe properly the interaction of the electrons with atoms of the target. For example, according to this model x-ray production for Cu Kα radiation in the Al matrix at 12 keV could not be calculated. The sphere of electron diffusion lies entirely below the surface of the target and no electron backscatter is predicated since electrons lose their critical energy before they can escape from the target. Although in this case contributions from large single elastic scattering are small, a model based on the diffusion theory is physically unrealistic. Experimentally, however, it is still possible to measure the distribution which has the usual shape.

The theoretical model based on the Transport Equation also fails to generate the $\phi(\rho z)$ curves which agree well with experimental $\phi(\rho z)$ curves. For example, this method gives x-ray absorption corrections which agree quite well with experimental data (the absorption correction is not too sensitive to the shape of $\phi(\rho z)$ curves) but fail to reproduce accurately the observed energy distribution of backscattered electrons. Thus this method cannot be used successfully for calculation of the atomic number effect. Furthermore, the $\phi(\rho z)$ curves have been calculated only for high electron energies (29 keV) and no attempts have been made to calculate the $\phi(\rho z)$ curves for low electron energies. Since the approximations made for calculating the $\phi(\rho z)$

curves (Rutherford cross section for scattering, continuous energy loss etc.) are more valid for high electron energies, it is expected that the $\phi(\rho z)$ curves for low electron energies, calculated according to this model, will be quite different from experimental $\phi(\rho z)$ curves. The major weakness of theory at present seems to lie in the somewhat questionable modeling of the scattering process.

The Monte Carlo method is so far the most physically satisfactory approach. But even this model gives the $\phi(\rho z)$ curves which fall short of the accuracy required for the atomic number corrections. Disagreement between measured and calculated $\phi(\rho z)$ curves is due to the various approximations. For instance, in the treatment of Bishop the Monte Carlo calculation is based on a simple screened Rutherford cross section and the Bethe continuous energy-loss equation. Neither of these expressions is very accurate, particularly for the heavy elements and low electron energies.

CHAPTER IV

Sample preparation

Sandwich samples consist of a thin layer of one element sandwiched in a matrix of a second element (Fig. 1). To obtain accurate measurements of the depth distribution of the x-ray production suitable for determining the atomic number effect, sandwich samples should fulfil following requirements:

1. The same tracer thickness in all matrix elements: The absolute value of intensity generated by the electron beam in the tracer layer depends on the thickness of the tracer layer. Different thicknesses of tracer layers in the sandwich samples of different matrix elements will make it impossible to determine the atomic number effect.

2. Uniform tracer thickness: Nonuniform tracer thickness over the area of a specimen will introduce errors to the measured x-ray intensities depending on position on the specimen.

3. Optimum tracer thickness: To obtain true shape of $\phi(\rho z)$ curves the thickness of the tracer layer should be infinitesimally thin. On the other hand the tracer has to be thick enough to yield measurable x-ray intensities. Choice of tracer layer thickness is a compromise between these two conflicting requirements.

4. Uniform, accurately known overlayer matrix thickness: The $\phi(\rho z)$ curve represents x-ray intensity generated by electron beam as a function of depth in the specimen. Any uncertainty in the determination of the thickness of the matrix layer as well as thickness variations lead to uncertainty in the depth at which the x-rays are generated. The result is to introduce uncertainty into the determination of the absorption correction as well as the atomic number correction through uncertainty in the area under the $\phi(\rho z)$ curve.

5. Freedom from fluorescence effects: Since we are interested only in the atomic number and absorption effects, any contribution to measured intensities due to the fluorescence gives the wrong depth distribution of x-ray production and hence incorrect absorption and atomic number corrections.

6. Easily evaporated elements: Because of the large number of evaporations required in the preparation of the sandwich samples, elements which can be easily evaporated from a hot tungsten filament are preferred.

Four samples were prepared for the measurement of the depth distribution curves. The matrix elements were aluminum, nickel, silver and gold and the tracer elements were silicon and copper. These two tracer elements were chosen to obtain the depth distribution

curves in two different regions of the x-ray spectra for the CuKα line at 8.98 KeV and SiKα line at 1.84 KeV. Also these elements give a very uniform thickness of the tracer layer. The matrix elements were chosen, in part, because of their x-ray properties, in part, because of the ease of evaporation. The matrix elements cover the Periodic Table from low atomic number, Al, to high atomic number, Au. This selection of tracer elements and matrix elements ensures that contributions due to the fluorescence of characteristic lines are insignificant.

The bases of the specimens were prepared in the following way. Four sections 3/8 inch thick were cut from a 3/4 inch diameter copper rod. Sheets approximately one millimeter thick of the matrix elements were attached to the copper by epoxy glue in the case of aluminum and by soldering in the cases of nickel, silver and gold. The edges of the sheets were removed to yield a substrate of the appropriate metal 3/4 inch in diameter. These speciments were rough polished using emery paper. Final polishing was done with 3 micron, then 1/4 micron diamond paste on microcloth using kerosene as lubricant. The surface of specimens was cleaned in a ultrasonic cleaner first using a soap water and then distilled water. The final cleansing step was to rinse the surface of specimens with ethyl alcohol and dry in air.

The vacuum evaporator used in preparation of the sandwich samples was of the standard type (Fig. 4) with mechanical forepump and oil diffusion pump. Liquid nitrogen was used in a cold trap during evaporation. The vacuum of the order of 10^{-6} torr was maintained during evaporation.

The most important factor in preparing the sandwich samples for these studies was to insure that the tracer element had exactly the same thickness in all four matrix elements. To insure uniformity of thickness during evaporation the four samples were rotated about their own axes and about an axis through the evaporation source. The copper was evaporated from a hot tungsten filament at a vacuum of better than 10^{-5} torr. The silicon was evaporated from a special tantalum boat.

The matrix elements were also evaporated from a hot tungsten filament. Masks were placed over the specimens to limit the area of deposition. By doubling the thickness of each successive matrix layer, 16 layers of different thickness can be deposited on a specimen in four evaporation (Fig. 5). By depositing one band perpendicular to 16 steps, 32 different thicknesses were prepared for each matrix element.

The elements were simultaneously deposited on the specimens, a glass slide and on an exposed area of a

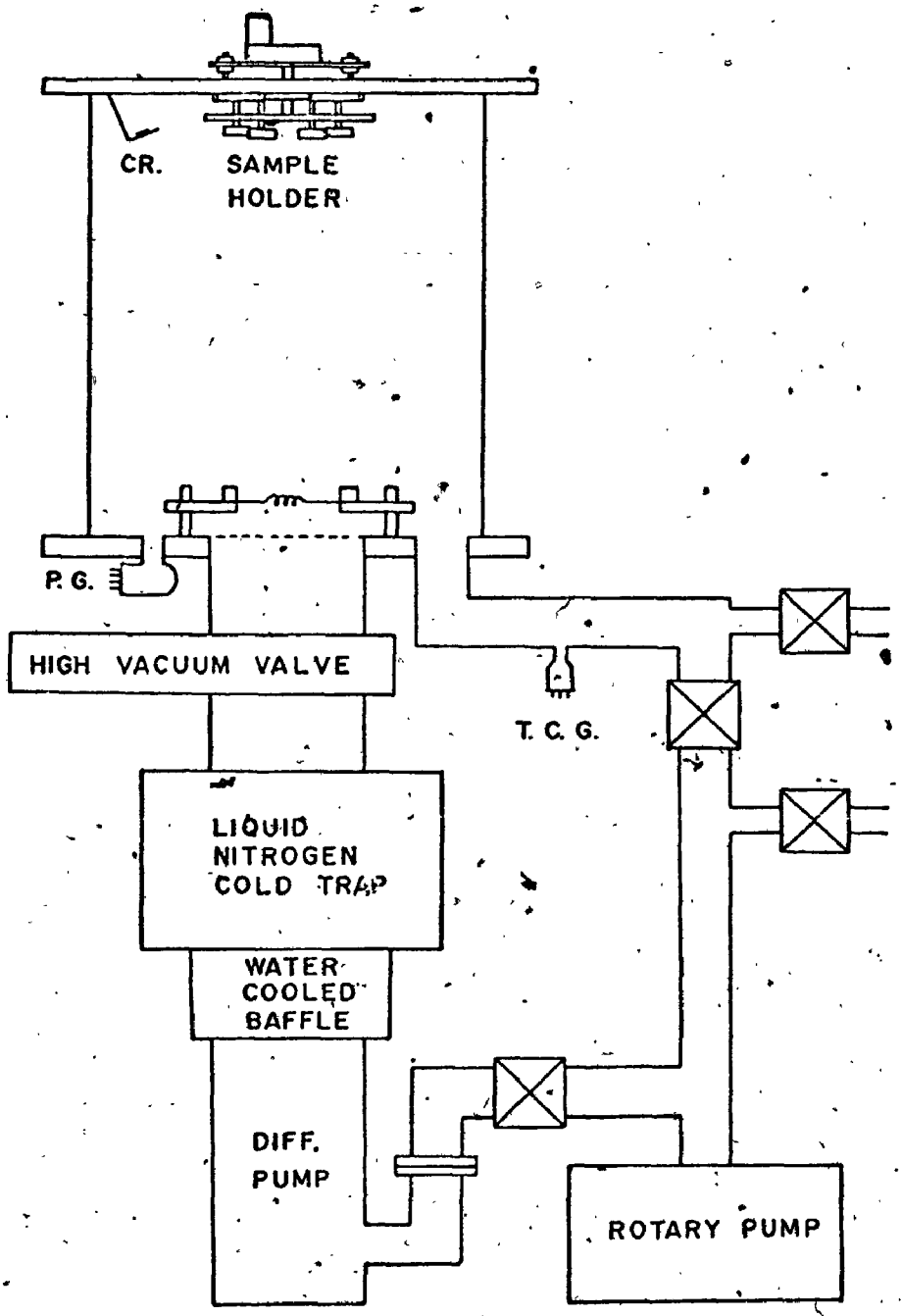

Figure 4. The Diagram of Vacuum Evaporator

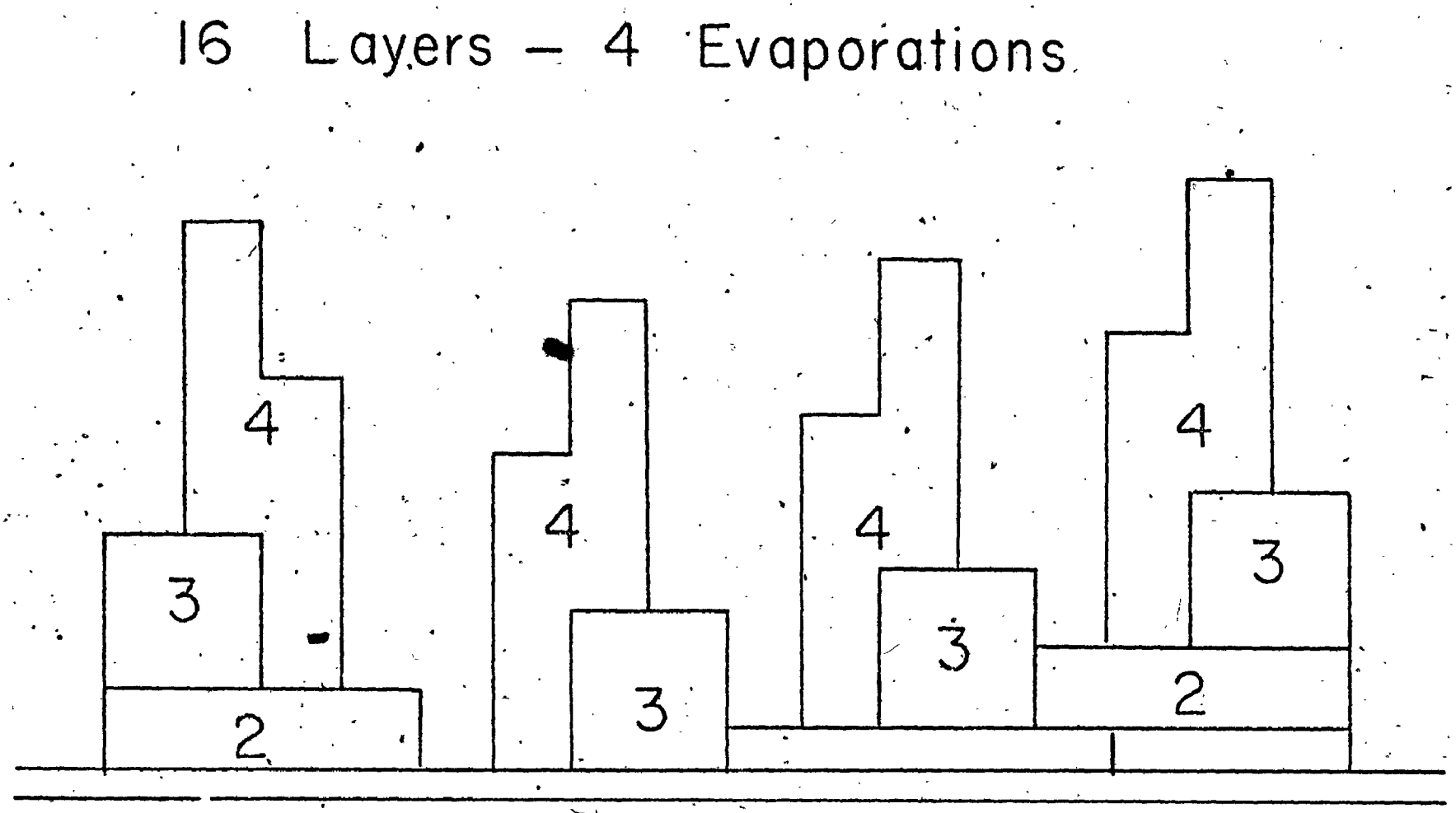

Figure 5. Sandwich Samples Used in this Thesis to Determine $\phi(\rho z)$ Curves

quartz crytal - monitor (Fig. 6). The absolute mass thickness of tracer and matrix layers were determined by weighing - as a weight difference of the glass slide before and after deposition. Since this method is not accurate enough for determining the mass thickness of thin layers (less than 40 $\mu g/cm^2$) the relative mass thickness of the deposited elements were also determined by using the quartz crystal monitor and by x-ray fluorescence spectrometry. The graphs (Fig.7-10) indicate the very good precision achieved in the determination of the mass thicknesses.(1) The mass thicknesses were determined, with relative errors of less than $\pm$ 2%. The thickness of the tracer layers for both Si and Cu is 4 $\mu g/cm^2$. No variation in thickness of deposited elements was observed.

The depth distribution curves were measured on a Cambridge Microscan 5 Electron Probe Microanalyser. The electron beam is perpendicular to the surface of the sample and x-ray take-off angle is 75°. Measurements have been made at 6,8 and 10 KeV for samples with a Si tracer and at 12 and 15 KeV for samples with a Cu tracer. A proportional flow counter with Mica crystal was used to detect SiKα radiation and the same counter with LiF crystal

---

(1) x-ray intensities have been corrected for background, dead time and absorption.

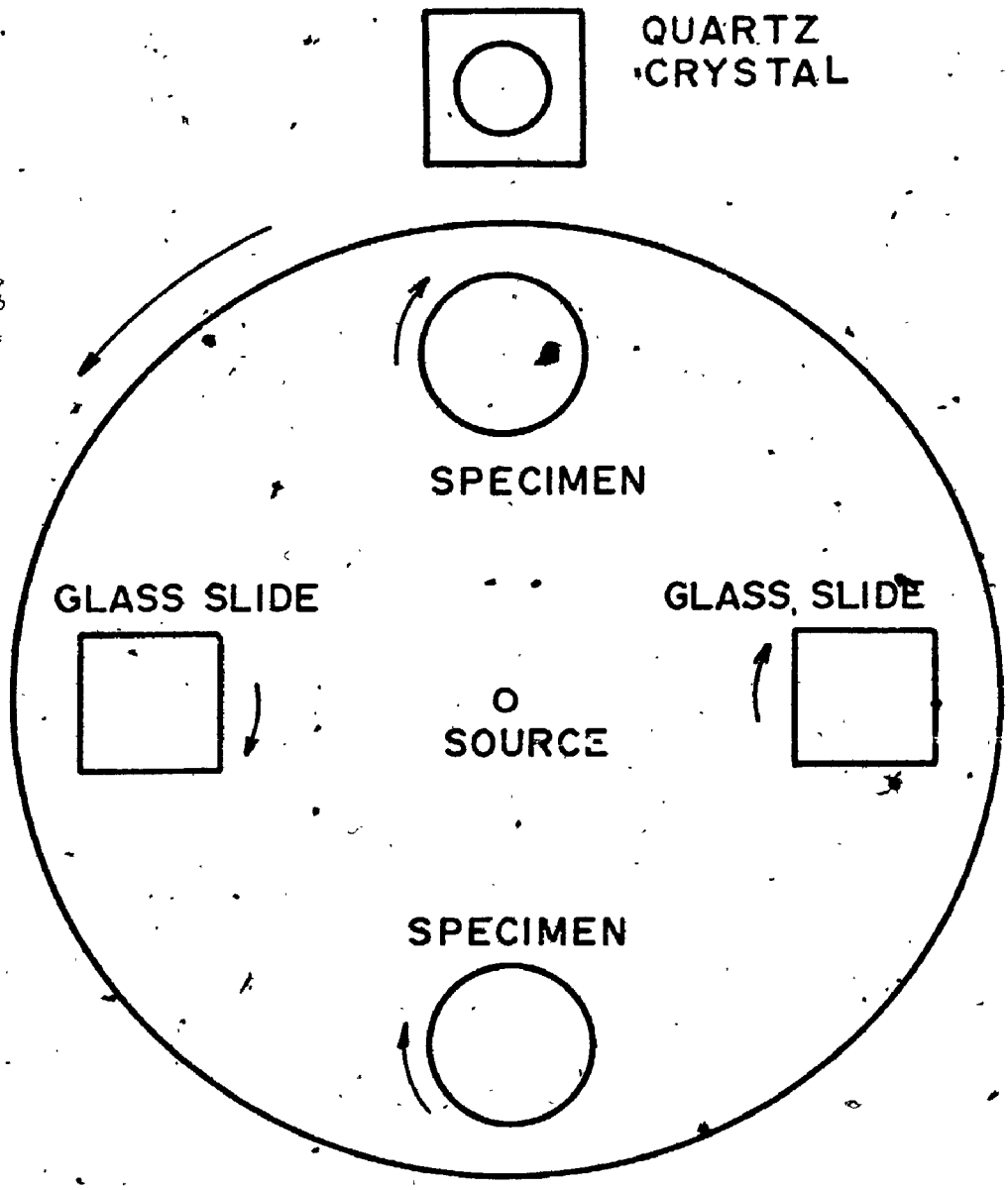

Figure 6. Diagram of the Sample Holder and Quartz Crystal Monitor Viewed from the Evaporation Source

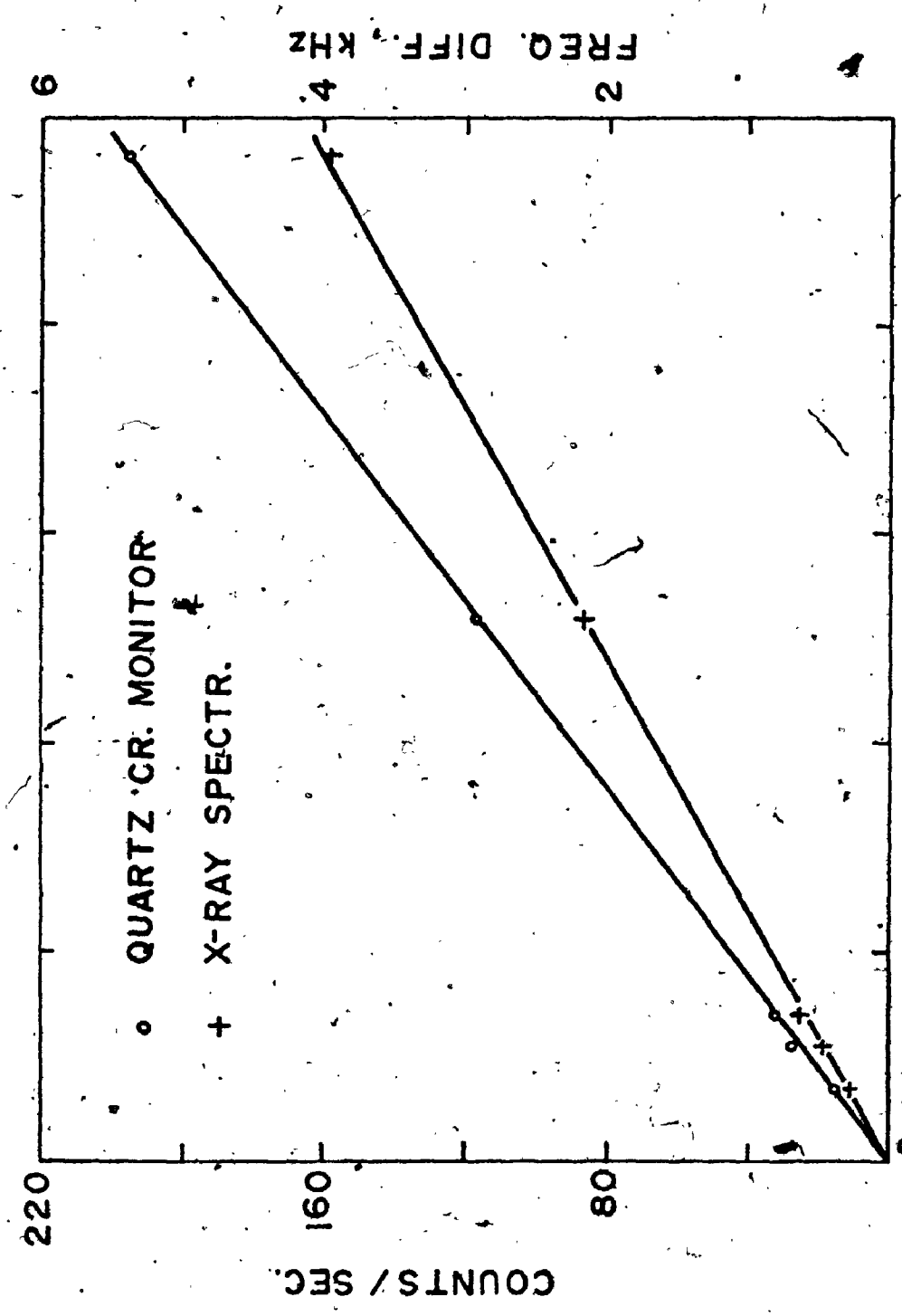

Figure 7. Calibration Curves for Aluminum

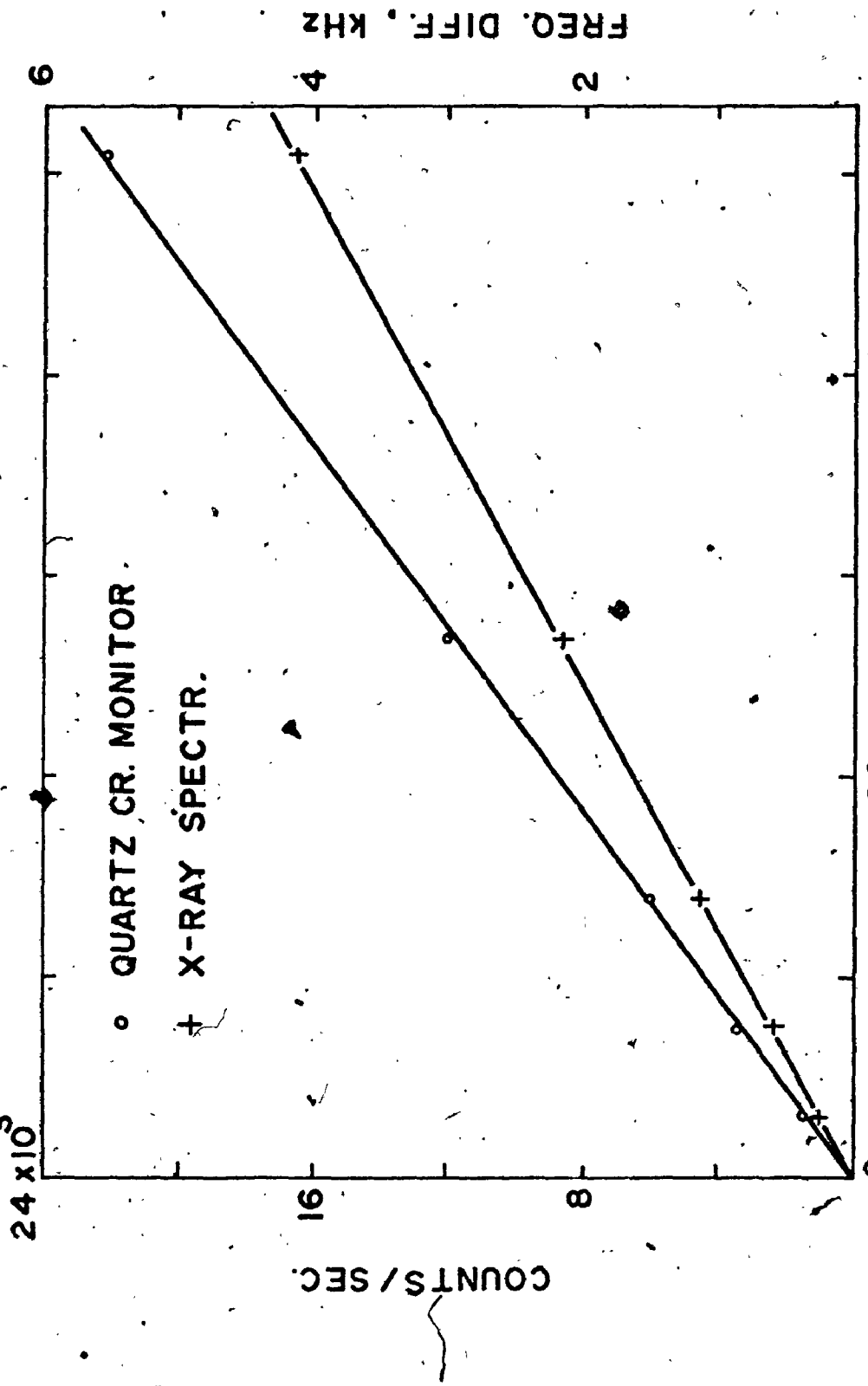

Figure 8. Calibration Curves for Nickel

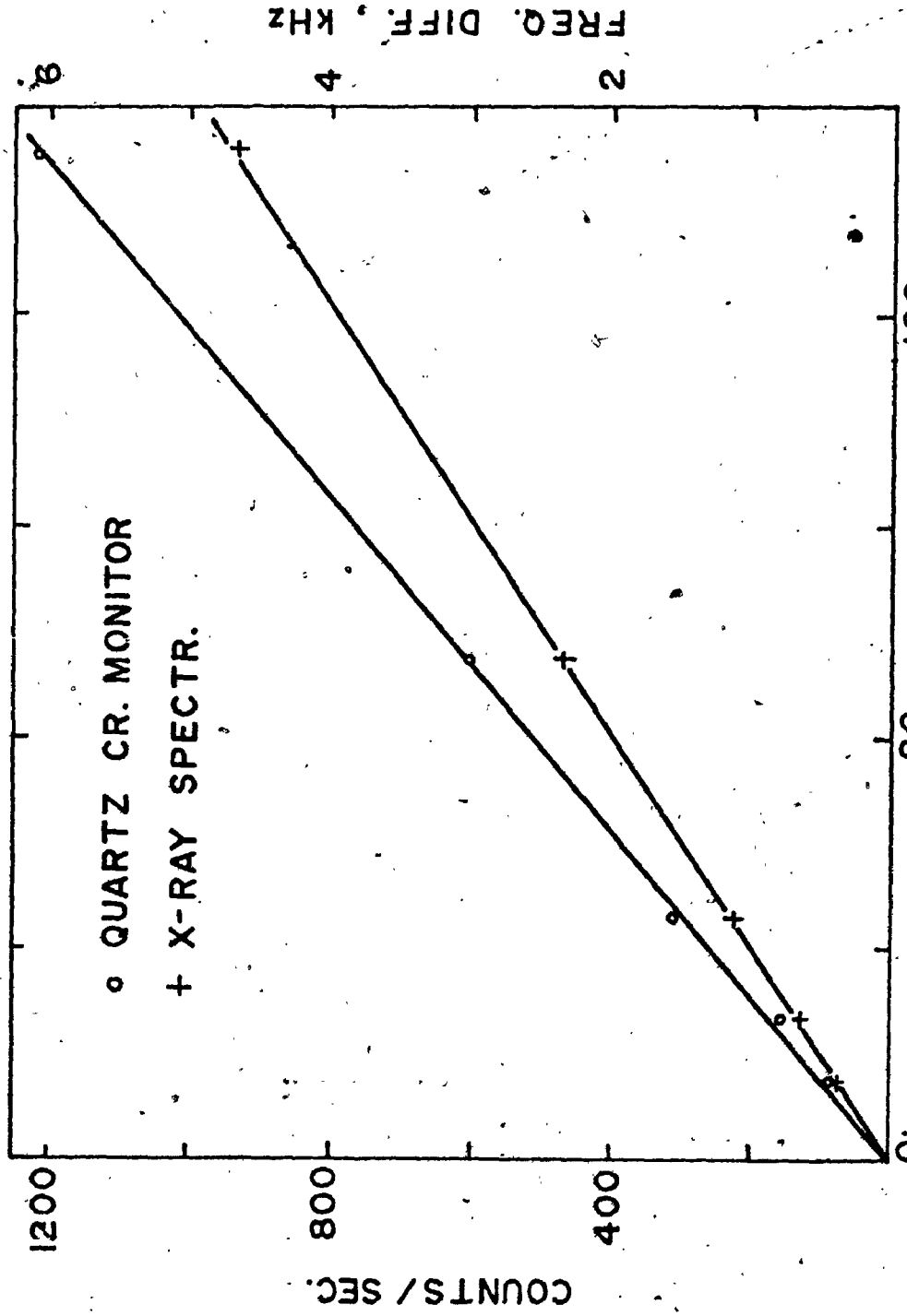

Figure 9. Calibration Curves for Silver

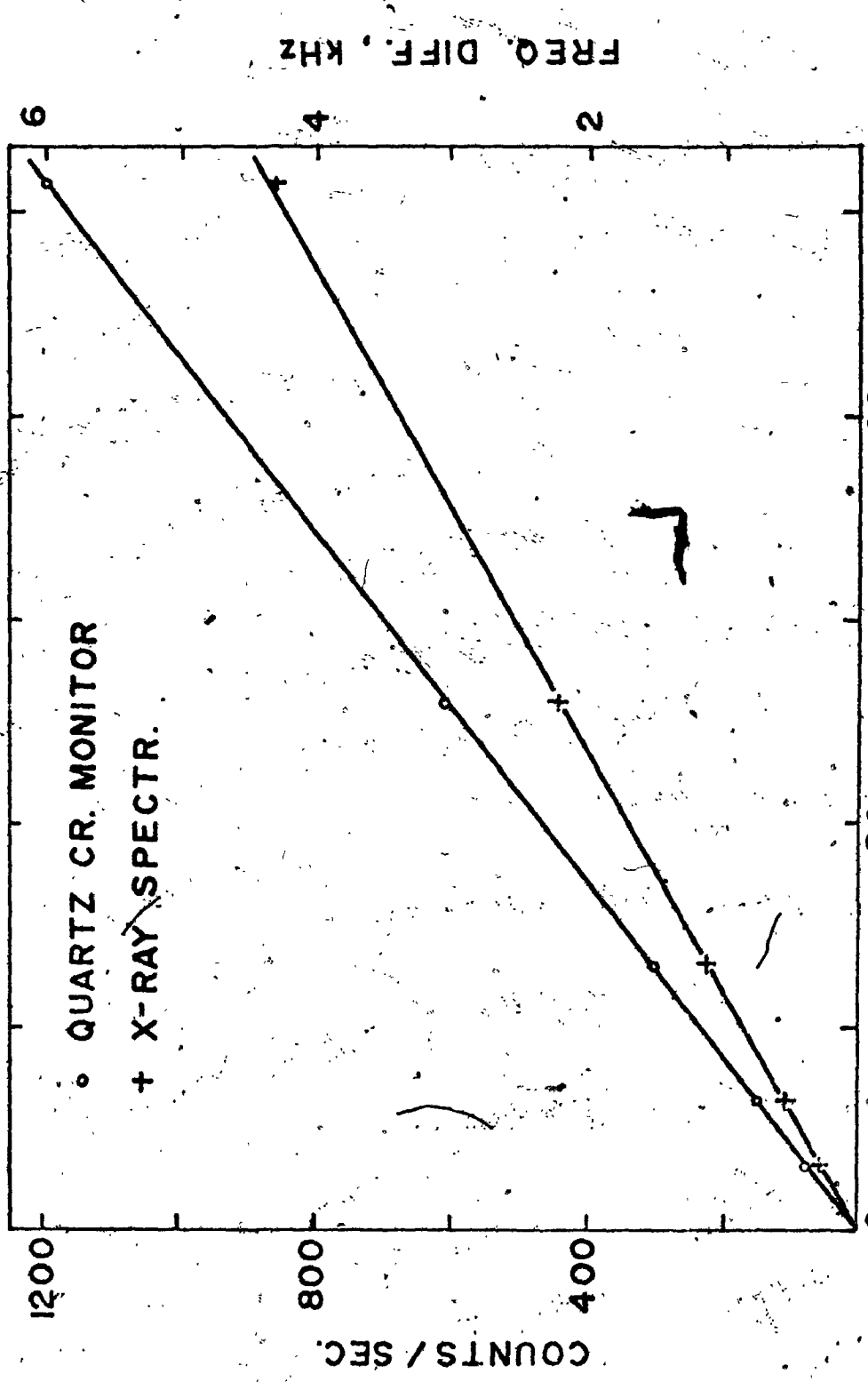

Figure 10. Calibration Curves for Gold

was used to detect CuKα radiation. Corrections were made to the data for dead time, background and absorption, using Heinrich's [45] values for mass absorption coefficients. The intensity from the standard pure element generally changed by less than 1% during the measurements from the sandwich samples which required as much as two hours.

Purity of the materials

The metals used for sample preparation were at least 99.9% pure. Any effects due to the 0.1% impurity in the tracer elements are too small to be detected at the level of precision of this work. The effect of any impurity in the matrix elements would similarly be negligible.

Statistical errors

To prevent carbon contamination of the specimen, the counting time from one spot has been limited to 20 seconds. Because of the low counting rate from the tracer layer as many as 20 intensity readings have been made on each of the layers in the sample. Typical x-ray intensities above background were of the order 16-40 counts per second.

The standard deviation, S_T for measurement of the number of random x-ray photons is given by the square root of the total number of counts, N_T,

$$S_T = \sqrt{N_T}$$

The total measured intensity is the sum of contribution from two sources, the actual x-ray intensity from atoms of the tracer, plus the background intensity. Thus a measurement of intensity from the tracer is subject to the statistical error inherent in two intensity determinations and the standard deviation S_N for a single measurement of the net intensity is

$$S_N = \sqrt{S_T^2 + S_B^2} = \sqrt{N_T + N_B}$$

where S_B and N_B are the values for the background measurements. The statistical error in the measurements is thus a function of the total counts accumulated for each of the intensity determinations which go to make up the value of $\phi(\rho z)$. The absolute error in $\phi(\rho z)$ decreases as N_T becomes smaller at greater depths in the sample, the percentage error, however, becomes larger.

Total intensities varied from 10-90 counts per second, depending on energy of incident electrons, type of radiation and matrix element. Taking the unfavorable case, a counting rate above background of 16 counts per second with a peak-to-background ratio of 4:1, 20 second counting times and 20 readings, the predicted standard deviation in the determination of $\phi(\rho z)$ is

$$S_\phi = \sqrt{(20 + 4)*20*20} = \sqrt{9600} = 98$$

This corresponds to 1.2% of the value of $\phi(\rho z)$.

If we now consider a point on the $\phi(\rho z)$ curve for which the net intensity is equal to the background intensity, then

$$S_\phi = \sqrt{(8 + 4)*20*20} = \sqrt{4800} = 69$$

Now, this standard deviation corresponds to about 2.2% of the value of $\phi(\rho z)$.

For determination of the atomic number correction is important to known areas under $\phi(\rho z)$ curves. The ratios of the area under $\phi(\rho z)$ curve for Si tracer and Al to areas under $\phi(\rho z)$ curves for Si tracer in Ni, Ag and Au respectively, represents the atomic number effect for SiKα radiation. Similarly the ratios of the area under $\phi(\rho z)$ curve for Cu tracer in Ni to the areas under $\phi(\rho z)$ curves for Cu tracer in Al and Ag respectively, represents the atomic number effect for CuKα radiation. To estimate an error in the determination of the area under the $\phi(\rho z)$ curve, the $\phi(\rho z)$ curve has been divided into sections $d\rho z$, each 10 $\mu g/cm^2$ wide. The standard deviation of the area under $\phi(\rho z)$ curve is then

$$\text{s.d. area} = \sqrt{\sum_{i=1}^{n} (S_{\phi_i} d\rho z_i)^2} \qquad (4\text{-}1)$$

where S_{ϕ_i} is standard deviation of the $\phi(\rho z)$ value in the section i. The standard deviation of the area

calculated according the formula (4-1) is about ± 3% in the case of Cu tracer in Al at 12 keV and Si tracer in Al at 6 keV. With increasing electron energy and atomic number the precentual error gradually decreases and is about ± 1.5% for Si tracer in Au at 10 keV and Cu tracer in Ag at 15 keV. There are also errors from other sources (numerical calculation of the area, fitting of the curves, etc.) but these errors are much less important.

Errors in Mass Absorption Coefficients

The mass absorption coefficients for CuKα radiation in Al, Ni and Ag and also mass absorption coefficients for SiKα radiation in Al, Ni, Ag and Au must be known for the exact determination of $\phi(\rho z)$ curves. For CuKα radiation (λ = 1.5405 Å) mass absorption coefficients in Al, Ni and Ag are relatively small and reasonably well known. Such is not the case for mass absorption coefficients for SiKα radiation (λ = 7.1253 Å) in Al, Ni, Ag and Au. For these elements the mass absorption coefficients are large and their values, because of the experimental difficulties in their determination, are not well known. The values of the mass absorption coefficients for SiKα radiation in Al, Ni, Ag and Au from different authors are shown in Table 2. In case of Al absorber, difference in the value of the mass

Table 2

Comparison of Mass Absorption Coefficients for SiKα Radiation in Al, Ni, Ag and Au.

Matrix	μ [cm^2/g] Henrich*	Theisen*	Kunz*
Al	3493	3634	3408
Ni	3152	3029	2929
Ag	2123	2086	2071
Au	1760	-	1737

* Henrich, K.F.J., The Electron Microprobe, 1966.

* Theisen, R. and Vollath, D., Tables of X-Ray Mass Absorption Coefficients, 1967.

* Kunz, F., Private Communication.

absorption coefficient between Heinrich's and Theisen values is more than 4%. Heinrich values of the mass absorption coefficients have been used in this work for calculation of $\phi(\rho z)$ curves.

CHAPTER V

The Experimental Results

The measured values of $\phi(\rho z)$ curves for the silicon tracer at the three electron energies and normal electron incidence are shown in Tables 3-6 for the aluminum, nickel, silver and gold matrices respectively. Similarly the $\phi(\rho z)$ values for a copper tracer at 15 and 12 kev are given in Tables 7, 8 and 9 for aluminum, silver and gold matrices. The curves plotted from these data are shown in Figures 11-17.

In the original work of Castaing, the values of $\phi(o)$, the intensity of x-rays generated at the surface of the sample (zero depth) was established on the basis of measurement of the intensity from the same thickness of tracer isolated in space. The $\phi(o)$ values reported in this thesis have not been established in this manner since the only important factor in establishing the absorption and the atomic number correction is $\phi(o)$ values for a given electron energy and x-ray wavelength on a relative basis. This can be done by taking the ratio of the intensities from the thin tracer layers on the surface of the various matrix elements to the intensity from the pure tracer element. However in order to compare curves with curves measured previously [56]

Table 3

$\phi(\rho z)$ Values - Si Tracer, Al Matrix
(Normal Electron Incidence)

Depth [$\mu g/cm^2$]	$\phi(\rho z)$ Values		
	10keV	8keV	6keV
0	1.390	1.350	1.290
12	1.781	1.600	1.479
20	1.836	1.651	1.382
26	1.907	1.708	1.310
34	1.928	1.739	1.055
40	1.913	1.687	0.973
48	1.862	1.580	0.768
62	1.801	1.391	0.435
102	1.446	0.711	0.102
124	1.146	0.368	0.031
130	1.157	0.358	0.020
138	0.959	0.266	
144	0.979	0.184	
152	0.898	0.164	
166	0.665	0.118	
191	0.507	0.031	
205	0.380		
219	0.193		
227	0.178		
233	0.172		
255	0.030		

Table 4

$\phi(\rho z)$ Values - Si Tracer, Ni Matrix
(Normal Electron Incidence)

Depth [$\mu g/cm^2$]	$\phi(\rho z)$ Values		
	10keV	8keV	6keV
0	1.670	1.580	1.460
11	2.083	2.033	1.767
28	2.345	2.004	1.258
41		1.855	1.018
54	2.204	1.537	0.682
67	2.126	1.493	0.514
84	1.845	1.050	0.235
97		0.838	0.192
105	1.524	0.645	
118	1.301	0.578	0.096
135	1.175	0.313	
148		0.332	
161	0.825	0.212	
174	0.714	0.241	
192	0.524	0.149	
202		0.111	
204	0.432	0.101	
232	0.257		
258	0.204		
288	0.121		
309	0.107		

Table 5

$\phi(\rho z)$ Values - Si Tracer, Ag Matrix
(Normal Electron Incidence)

Depth [$\mu g/cm^2$]	$\phi(\rho z)$ Values		
	10keV	8keV	6keV
0	1.840	1.740	1.620
13	2.408	2.168	1.917
25	2.544	2.206	1.711
40	2.525	2.129	1.385
44	2.520	1.973	1.217
59	2.468	1.688	0.891
72	2.262	1.455	0.637
86	2.108	1.179	0.451
93	2.070	1.250	0.455
108	1.797	1.084	0.273
120	1.696	0.818	0.177
135	1.394	0.604	0.086
139	1.404	0.679	0.038
154	1.236	0.418	0.019
166	1.045	0.299	0.024
181	0.824	0.295	
189	0.843	0.252	
204	0.680	0.176	
216	0.609	0.128	
231	0.465	0.095	
235	0.469		
250	0.340		
262			
277	0.273		

Table 6

$\phi(\rho z)$ Values - Si Tracer, Au Matrix
(Normal Electron Incidence)

Depth [$\mu g/cm^2$]	$\phi(\rho z)$ Values		
	10keV	8keV	6keV
0	2.060	1.960	1.830
11	2.620	2.340	2.032
24	2.700	2.315	1.739
37		2.135	1.517
50	2.560	1.995	1.203
63	2.470	1.835	1.041
76	2.380	1.650	0.753
89	2.245	1.510	0.506
102	2.030	1.270	0.500
115	1.935	1.235	0.334
128	1.770	0.950	0.313
141	1.545	0.800	0.167
154	1.390	0.660	0.192
167	1.240	0.515	0.086
180	1.110	0.460	0.071
193	0.940	0.435	
204	0.960	0.370	
217		0.250	
230	0.680	0.260	
256	0.480	0.115	
282	0.415		
295		0.100	
308	0.320		
334	0.260		
360	0.220		
386	0.150		
399	0.075		

Table 7

$\phi(\rho z)$ Values for Cu Tracer in Al Matrix
(Normal Electron Incidence)

Depth [$\mu g/cm^2$]	$\phi(\rho z)$ Values	
	15 keV	12 keV
0	1.150	1.100
12	1.234	1.172
20	1.255	1.157
26	1.338	1.203
34	1.302	
40		1.126
48	1.307	1.100
62		0.894
102	1.275	0.586
124	1.134	0.386
126	1.108	
130	1.166	0.359
138	1.139	0.272
144	1.004	0.242
152	1.045	0.206
166	0.810	
191	0.758	0.067
205	0.685	
213	0.580	
219	0.596	
227	0.585	
233	0.512	
241	0.486	
255	0.376	
295	0.277	
317	0.188	
319	0.188	
323	0.209	
331	0.157	
337	0.125	
345	0.146	

Table 8

$\phi(\rho z)$ Values - Cu Tracer, Ni Matrix
(Normal Electron Incidence)

Depth [$\mu g/cm^2$]	$\phi(\rho z)$ Values	
	15keV	12keV
0	1.370	1.230
11	1.630	1.400
28	1.670	1.340
41	1.830	1.375
54		1.280
67	1.800	1.210
84	1.660	0.990
97	1.650	0.795
105	1.470	0.715
118	1.500	0.575
135	1.210	0.400
148	1.350	0.335
161	1.115	0.275
174	1.025	0.215
191	0.860	0.165
202	0.760	0.080
215	0.750	
232	0.500	
245	0.580	
258	0.455	
271	0.420	
288	0.320	
309	0.210	
322	0.200	
352	0.230	
365	0.105	
395	0.040	
408	0.100	

Table 9

$\phi(\rho z)$ Values for Cu Tracer in Ag Matrix
(Normal Electron Incidence)

Depth [$\mu g/cm^2$]	$\phi(\rho z)$ Values	
	15keV	12keV
0	1.580	1.370
13	1.840	1.500
25	1.940	1.560
40	1.860	1.480
44	1.950	1.480
59	1.915	1.300
71	1.835	1.280
86	1.790	1.085
93	1.790	1.070
108		0.910
120	1.590	0.820
135	1.480	0.760
139	1.370	0.600
154	1.450	0.555
166	1.200	0.430
181	1.200	0.400
189	1.005	0.300
204	1.000	0.320
216	0.905	0.160
231	0.800	0.125
235	0.650	
250	0.740	
262	0.610	
277	0.590	
284	0.480	
299	0.480	
315	0.360	
326	0.420	
330	0.270	
345	0.325	
357	0.220	
372	0.240	

$\phi(o)$ values have been estimated from Hutchin's [61] data at each voltage for the silicon tracer in the aluminum matrix and for the copper tracer in the nickel matrix. For the other matrices, the $\phi(o)$ values are based simply on relative intensity measurements from the thin layer at the surface from one matrix element to the intensity measured under identical conditions from another matrix element. Thus the absolute values depend on Hutchin's data, but relative values at any given voltage should be correct to the limits of the experimental errors of this work.

Some characteristics of the depth distributions Fig. 11-17 are readily apparent. The depth of maximum x-ray production decreases as the atomic number of the matrix element increases. The same trend is evident both for SiKα and also for CuKα radiation. One of the interesting aspects of the depth distribution curves is the large increase which occurs between the $\phi(o)$ value and the maximum in the depth distribution at low electron energies. Earlier curves, reported in the literature [10,56], tend to show that as the electron energy decreases the increase from the $\phi(\rho)$ value to the maximum in the $\phi(\rho z)$ curve becomes less and less. The apparent reason for this decrease is the loss in definition because of the significant thickness of tracer layer used in previous measurements. For example, for

2 2

OF/DE

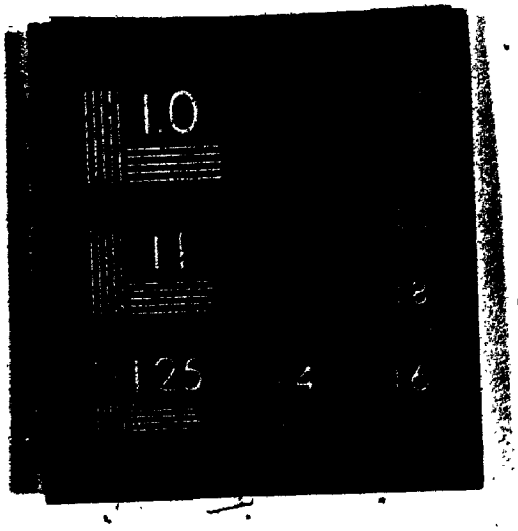

the silicon tracer, the increase from $\phi(o)$ to the maximum in the curve represents 40% at 10keV, 27% at 8keV and 21% at 6keV for the nickel matrix. Thus the major effect in the production of the maximum in the curves must be the diffusion of electrons rather than the increased efficiency of x-ray production as the electron energy degrades towards the absorption edge energy.

Absorption Correction Curves

Once the depth distribution of x-ray production is known, the fraction of x-rays which will escape from the sample as a function of the absorption parameter χ can be readily calculated for all values of χ. Tables 10 and 11 give $f(\chi)$ values calculated from the depth distribution curves. Figure 18 shows one set of such curves for the silicon tracer and nickel matrix at three electron energies and Figure 19 shows $f(\chi)$ curves for Si tracer and Al, Ni, Ag and Au matrices at an electron energy of 8keV. The most popular expression for appoximating the absorption correction is that of Philibert using the modification of Duncumb and Shields to allow for the x-ray excitation energy and the electron absorption parameter σ of Heinrich. A comparison has been made between the $f(\chi)$ curves obtained form $\phi(\rho z)$ curves reported in this thesis and the values obtained by calculation from

the Philibert formula. A selected comparison of these values is shown in Table 12. In this table differences exist between the $f(\chi)$ values generated in this study and those calculated from the Philibert expression. These differences are as much as 2% even for $f(\chi)$ values of 0.9 and greater. Thus some changes still need to be made to the Philibert expression to properly allow for the matrix and energy dependance of the absorption correction of low electron energies.

The Atomic Number Effect

Since the depth distrubtions have been measured with identical tracer layer thicknesses and different matrices, integration of the area under the curves for different matrix elements yields directly the atomic number effect. This is given by the expression

$$\text{At. No. Correction Factor} = \frac{\int_0^\infty \phi_{AB}(\rho z)\, d(\rho z)}{\int_0^\infty \phi_A(\rho z)\, d(\rho z)}$$

and then in the absence of the fluorescence effect

$$\frac{I'_{AB}}{I'_A} = C_A \text{ (At. No. Corr. Factor)}$$

where I'_{AB} and I'_A are x-ray intensity directly generated in the sample (primary intensity) and the pure element standard respectively.

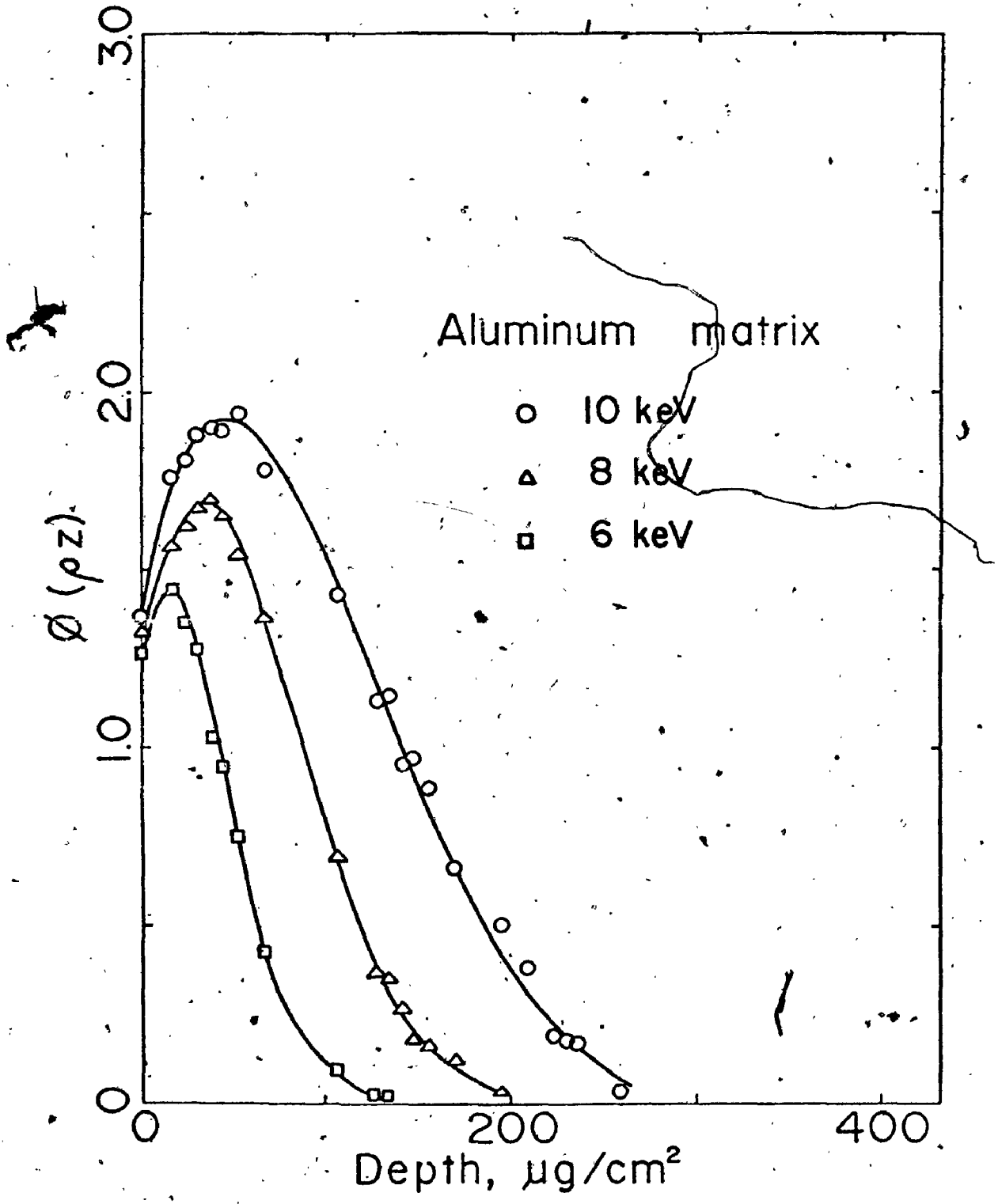

Figure 11. Measured $\phi(\rho z)$ Curves for a Si Tracer in Aluminum

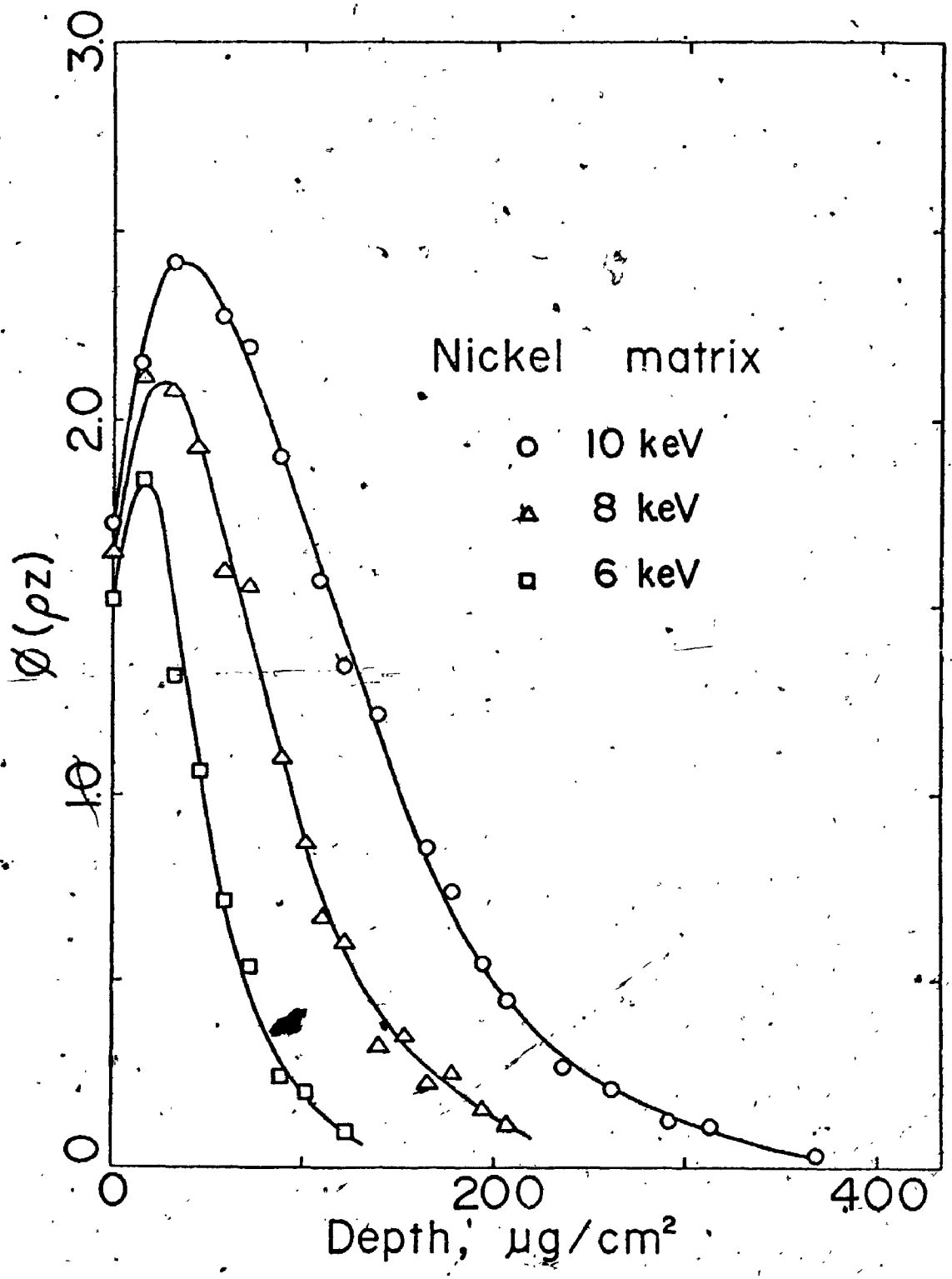

Figure 12. Measured $\phi(\rho z)$ Curves for a Si Tracer in Nickel

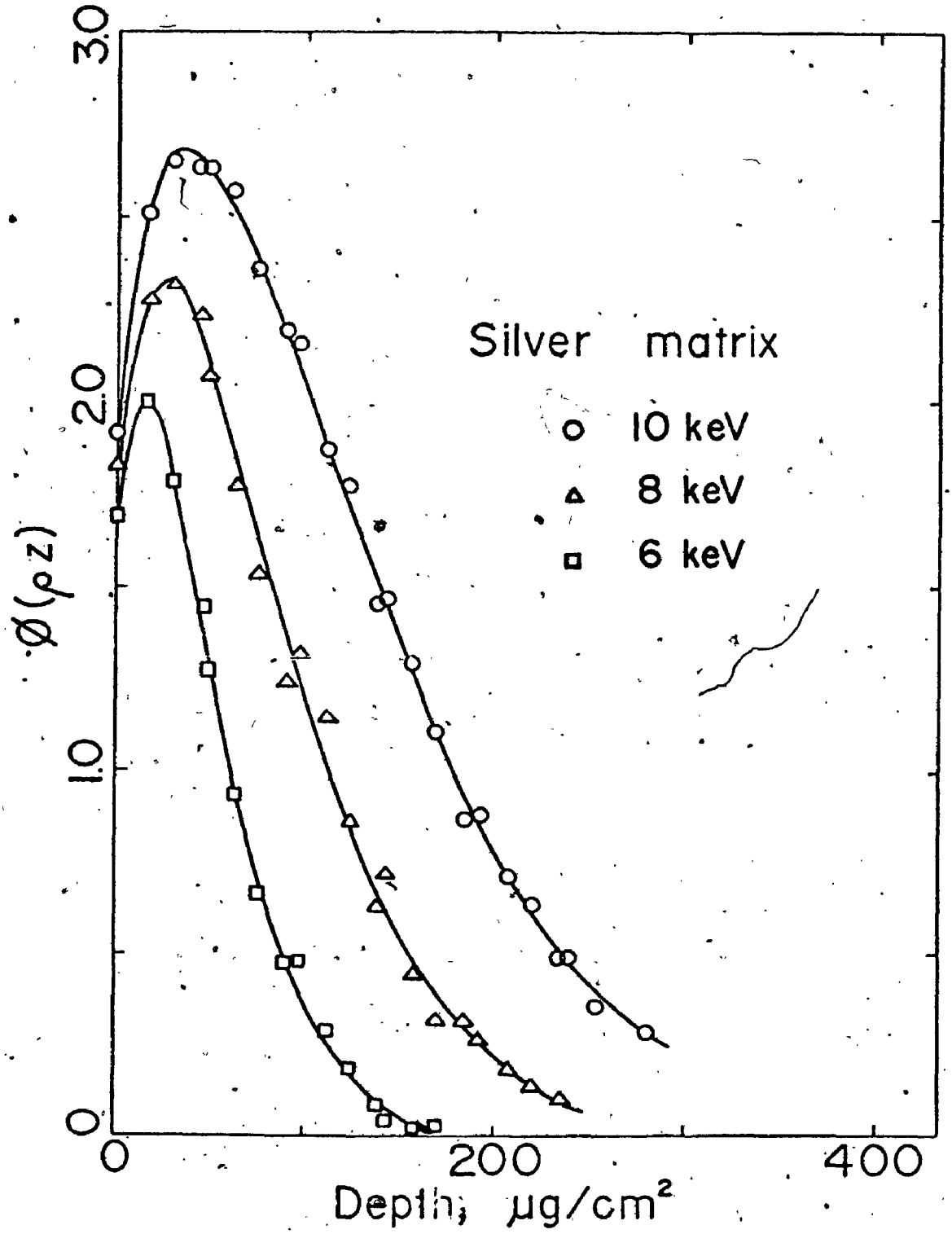

Figure 13. Measured $\phi(\rho z)$ Curves for a Si Tracer in Silver

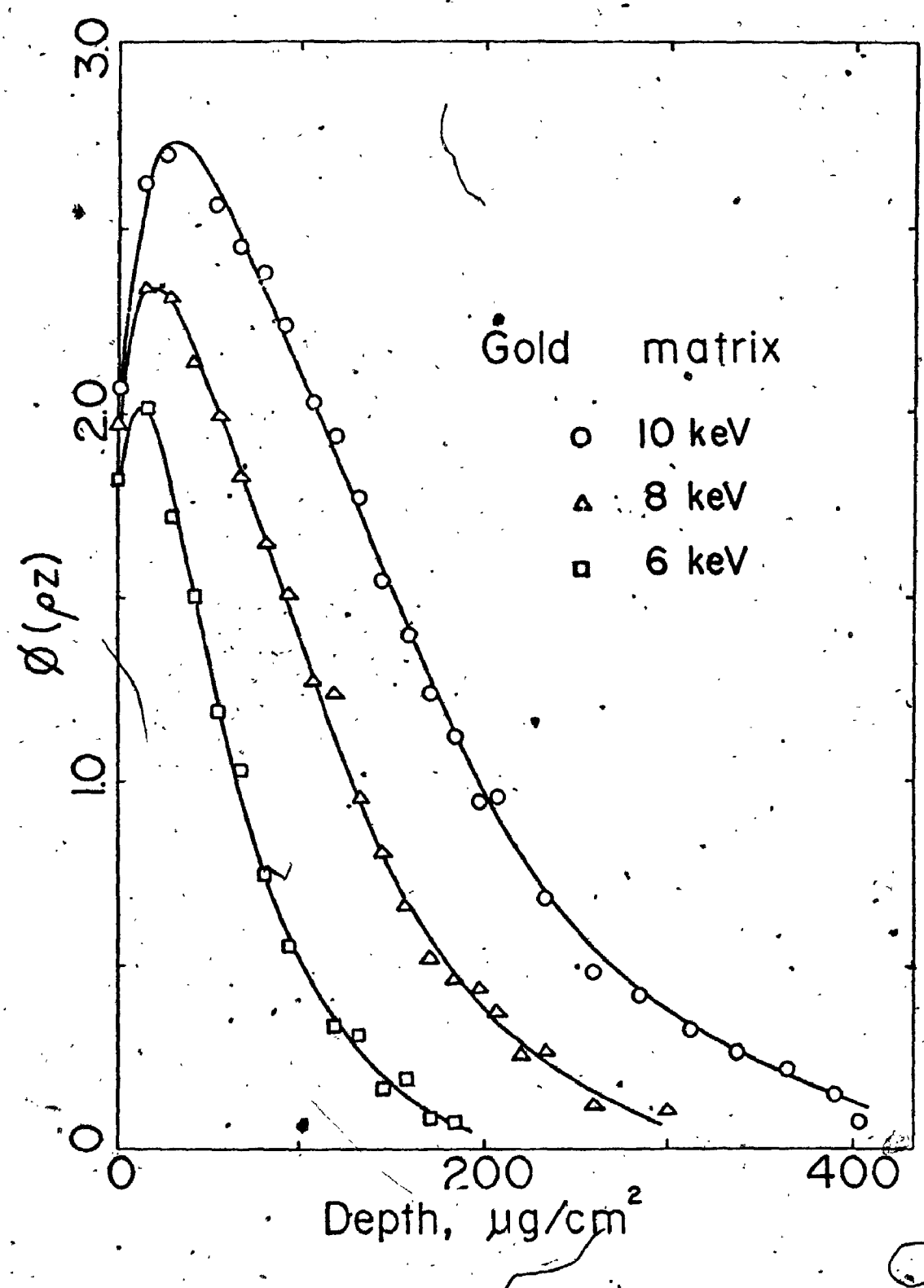

Figure 14. Measured $\phi(\rho z)$ Curves for a Si Tracer in Gold

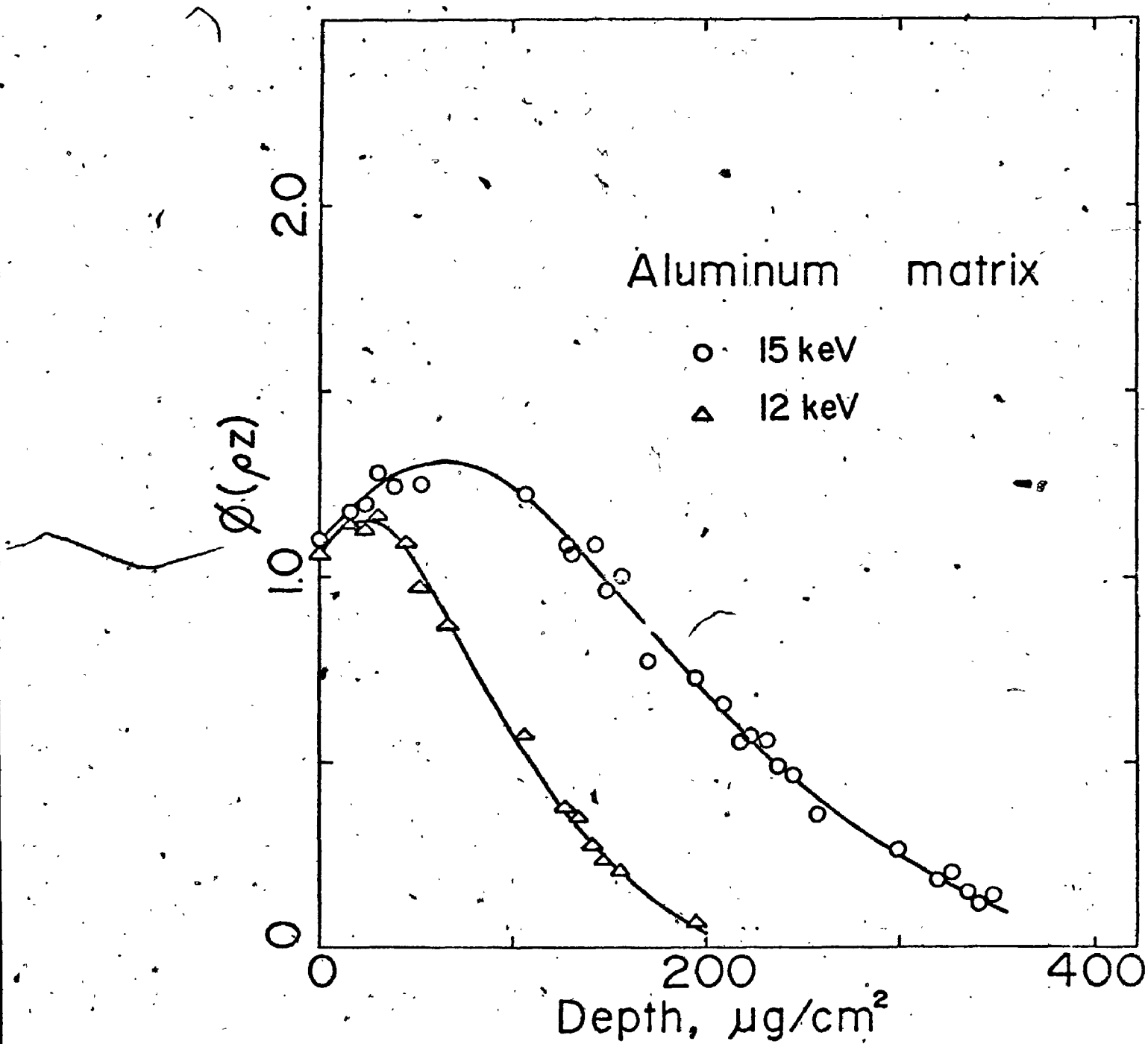

Figure 15. Measured $\phi(\rho z)$ Curves for a Cu Tracer in Aluminum

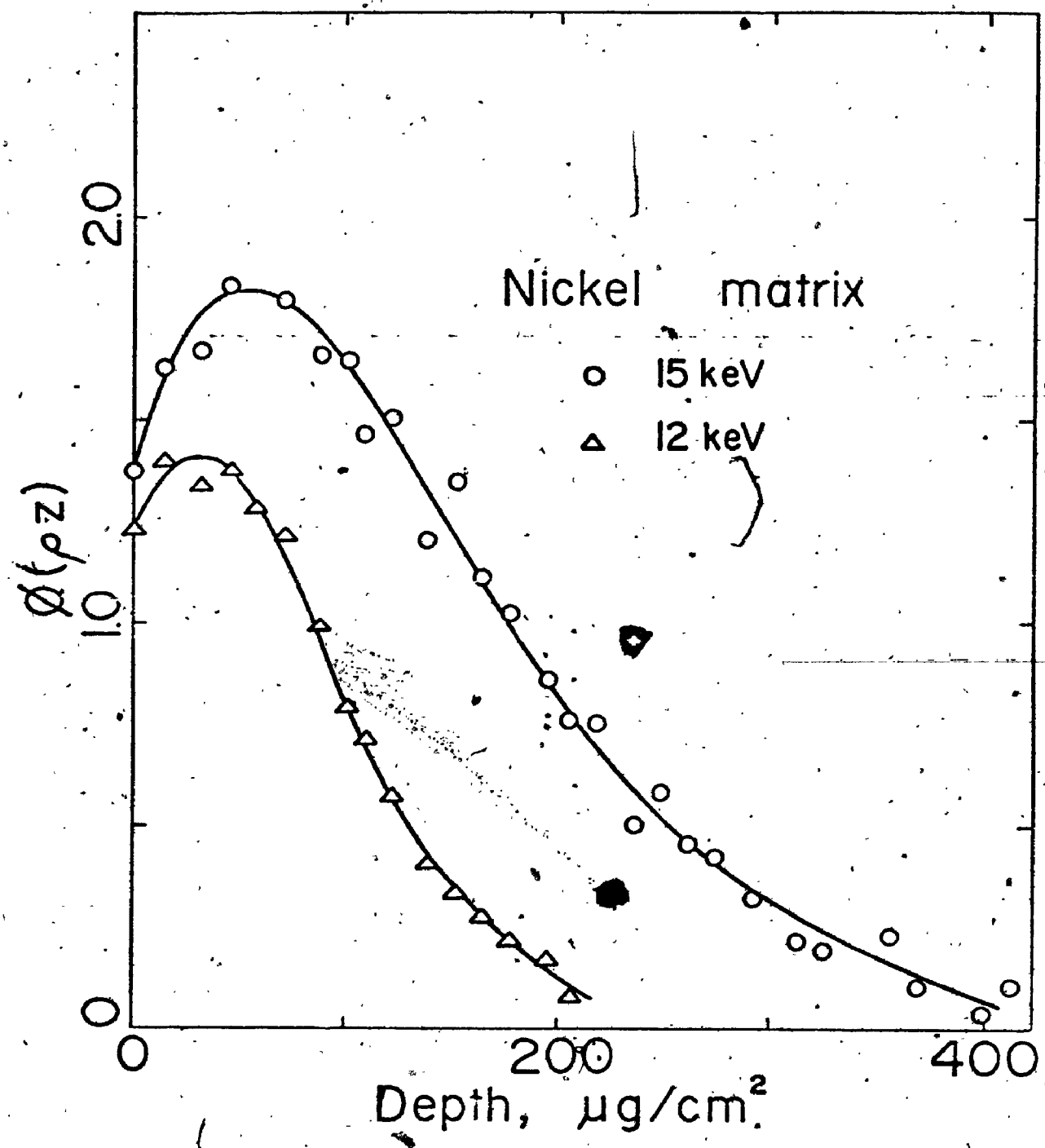

Figure 16. Measured $\phi(\rho z)$ Curves for a Cu Tracer in Nickel

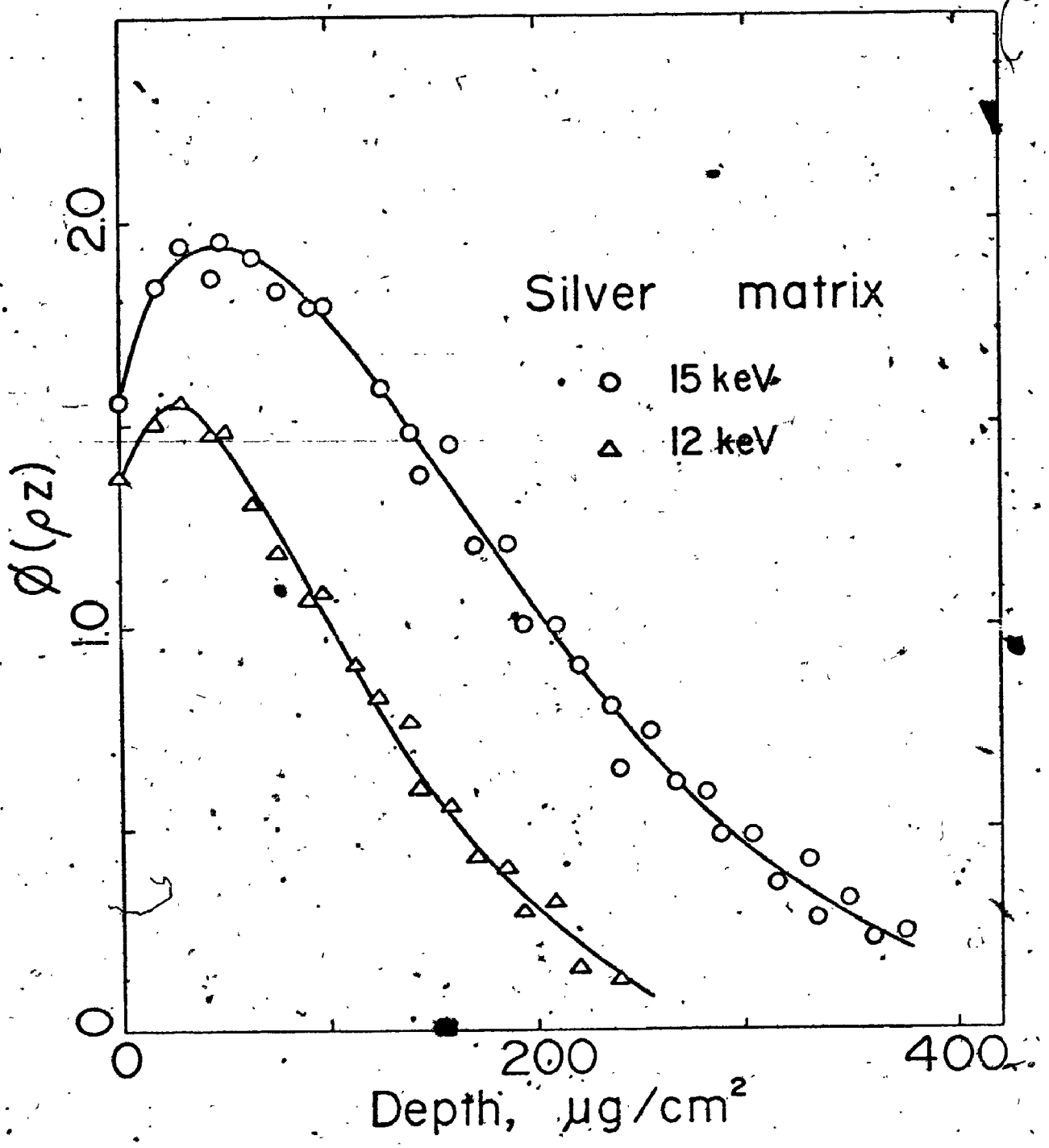

Figure 17. Measured $\phi(\rho z)$ Curves for a Cu Tracer in Silver

Table 10

The f(χ) Values Determined from φ(ρz) Curves for SiKα Radiation at Electron Energy of 8keV

χ[cm²/g]	Matrix			
	Al	Ni	Ag	Au
40	0.998	0.997	0.997	0.997
80	0.995	0.995	0.994	0.993
120	0.993	0.992	0.991	0.990
160	0.991	0.990	0.989	0.987
200	0.988	0.987	0.986	0.983
300	0.982	0.981	0.979	0.975
400	0.977	0.974	0.972	0.967
500	0.971	0.968	0.965	0.959
600	0.965	0.962	0.958	0.951
700	0.960	0.956	0.951	0.944
800	0.954	0.950	0.945	0.936
900	0.949	0.944	0.938	0.928
1000	0.943	0.938	0.931	0.921
1200	0.932	0.926	0.919	0.906
1400	0.922	0.915	0.906	0.892
1600	0.911	0.904	0.894	0.878
1800	0.901	0.893	0.882	0.865
2000	0.891	0.882	0.870	0.852
2500	0.867	0.856	0.842	0.820
3000	0.843	0.831	0.815	0.790
3500	0.821	0.807	0.789	0.762
4000	0.799	0.785	0.765	0.736
4500	0.778	0.763	0.742	0.711
5000	0.758	0.742	0.720	0.688

Table 11

The f(χ) Values Determined from φ(ρz) curves for SiKα Radiation

	Ni Matrix		
χ[cm²/g]	10keV	8keV	6keV
40	0.996	0.997	0.998
80	0.992	0.995	0.997
120	0.989	0.992	0.995
160	0.985	0.990	0.994
200	0.981	0.987	0.993
300	0.972	0.981	0.989
400	0.963	0.974	0.985
500	0.954	0.968	0.981
600	0.945	0.962	0.978
700	0.937	0.956	0.974
800	0.928	0.950	0.971
900	0.920	0.944	0.967
1000	0.912	0.938	0.963
1200	0.895	0.926	0.956
1400	0.880	0.915	0.949
1600	0.864	0.904	0.942
1800	0.849	0.893	0.936
2000	0.835	0.882	0.929
2500	0.800	0.856	0.912
3000	0.768	0.831	0.896
3500	0.738	0.807	0.881
4000	0.710	0.785	0.866
4500	0.683	0.763	0.851
5000	0.658	0.742	0.831

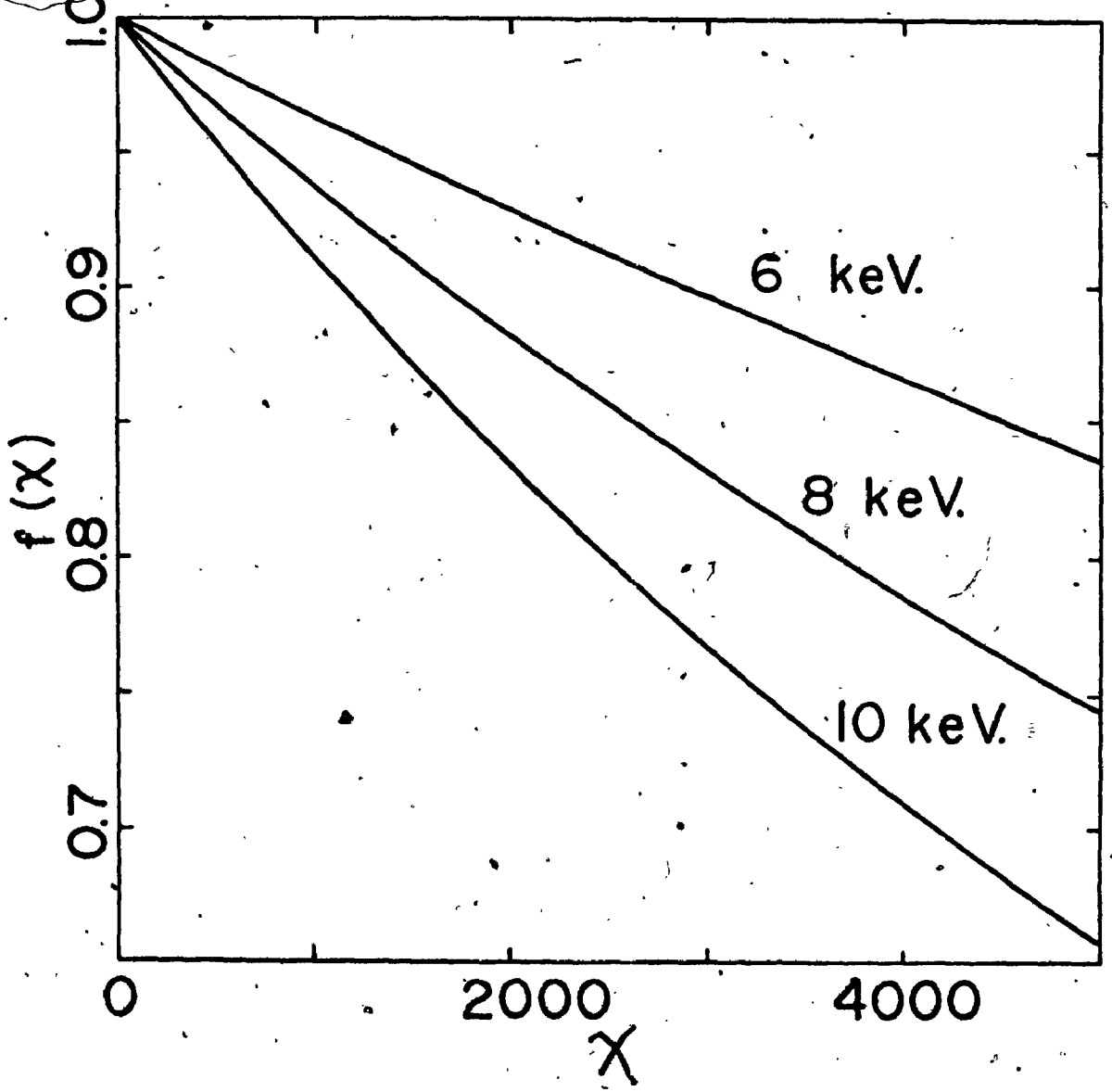

Figure 18. The f(χ) Curves Obtained from φ(ρz) Curves and for a Si Tracer and Ni Matrix at 10, 8 and 6keV

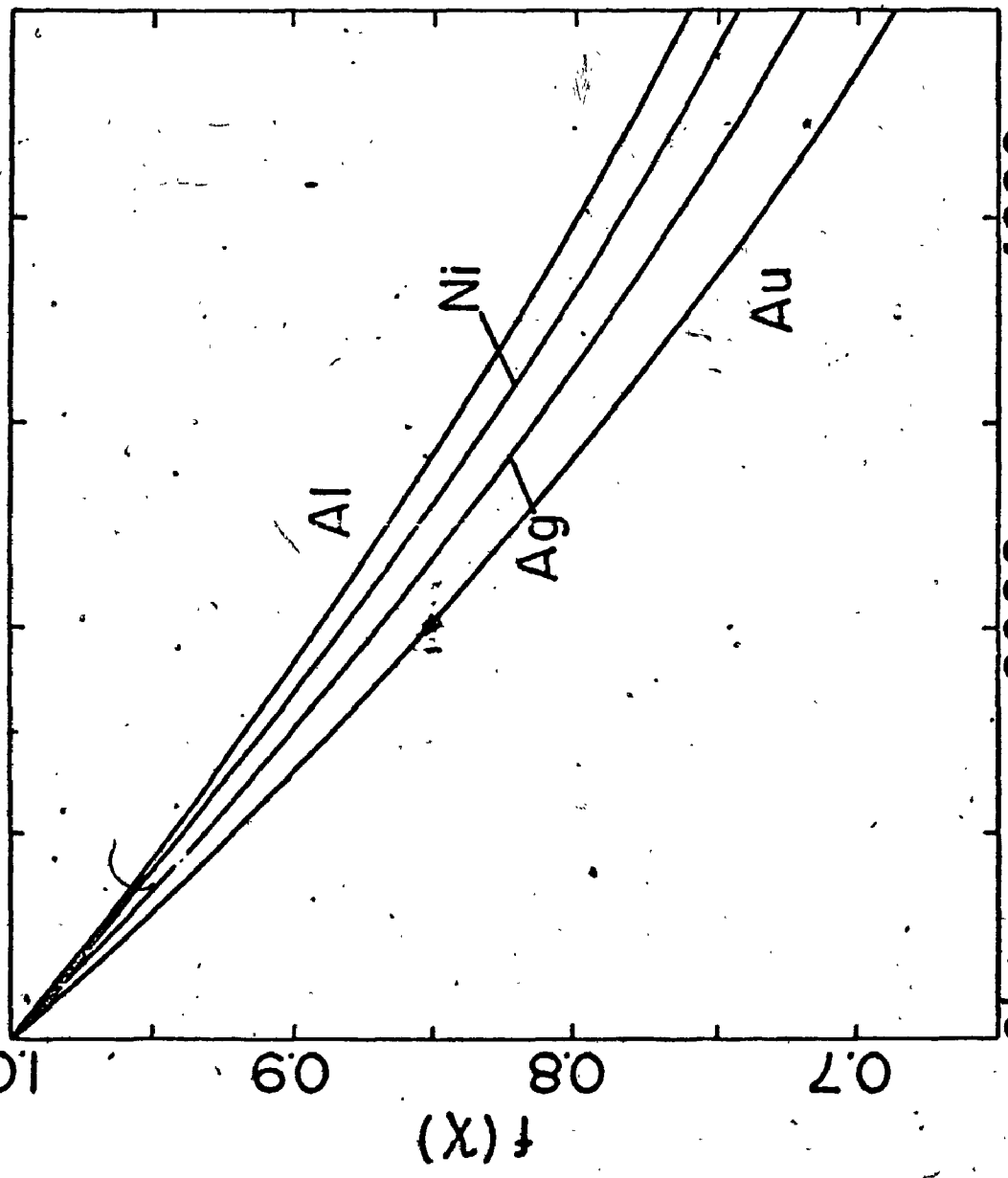

Figure 19. The f(χ) Curves Obtained from φ(ρz) Curves for a Si Tracer in Al, Ni, Ag and Au at an electron energy of 8keV

The atomic number correction as determined from the area under $\phi(\rho z)$ curves is given in Table 13 for SiKα and CuKα radiation. These data show that as the atomic number of the matrix increases, the number of x-rays generated per incident electron also increases. These values of the atomic number effect are appropriate for the situation where there is a small concentration of the tracer element in a sample which is essentially 100% of the matrix element. The advantage of using such depth distribution curves for calculating the atomic number effect lies in the complete separation of the atomic number effect from the aborption correction. Thus measurements of this kind yield the direct measurement of the atomic number effect in an unambiguous fashion. Comparison can be made with the methods of calculation of the atomic number effect reported in the Chapter II. Table 14 shows a comparison of atomic number correction factors obtained by the sandwich sample technique, the Duncumb and Reed method and by the Diffusion Model modified by Wolf and Macres.

The difference between atomic number correction factors calculated according to Diff. Model and those derived from $\phi(\rho z)$ curves is large. This was expected since the Diff. Model does not adequately describe the interaction of electrons with solids. On the other hand values

Table 12

Comparison of f(χ) Values Obtained from φ(ρz) Curves and From Philibert Formula

Si Tracer, 8keV

	Matrix							
	Al		Ni		Ag		Au	
χ	φ(ρz)	Philibert	φ(ρz)	Philibert	φ(ρz)	Philibert	φ(ρz)	Philibert
200	0.9882	0.9849	0.9871	0.9858	0.9856	0.9862	0.9833	0.9864
500	0.9710	0.9628	0.9682	0.9653	0.9647	0.9661	0.9591	0.9667
1000	0.9432	0.9279	0.9380	0.9327	0.9314	0.9344	0.9209	0.9356
2000	0.8911	0.8645	0.8819	0.8734	0.8699	0.8765	0.8515	0.8787
5000	0.7582	0.7130	0.7424	0.7311	0.7197	0.7375	0.6876	0.7421

Si Tracer, 6keV

	Matrix							
	Al		Ni		Ag		Au	
χ	φ(ρz)	Philibert	φ(ρz)	Philibert	φ(ρz)	Philibert	φ(ρz)	Philibert
200	0.9930	0.9911	0.9925	0.9917	0.9913	0.9919	0.9895	0.9920
500	0.9826	0.9979	0.9814	0.9794	0.9784	0.9799	0.9742	0.9803
1000	0.9657	0.9567	0.9634	0.9596	0.9576	0.9606	0.9494	0.9613
2000	0.9332	0.9165	0.9289	0.9221	0.9181	0.9240	0.9030	0.9253
5000	0.8453	0.8121	0.8366	0.8243	0.8138	0.8286	0.7844	0.8316

Table 13

Experimental Values of the Atomic Number Correction for SiKα and CuKα Radiation in Al, Ni, Ag and Au Matrix

SiKα

Eo[keV]	Al	Ni	Ag	Au
10	1.000	1.180	1.398	1.750
8	1.000	1.196	1.430	1.810
6	1.000	1.220	1.510	1.920

CuKα

Eo[keV]	Al	Ni	Ag
15	0.800	1.000	1.180
12	0.775	1.000	1.250

Table 14

Comparison of Atomic Number Correction Obtained by the Sandwich Technique, the Duncumb and Reed Equation and Diff. Model Calculations

SiKα

	Ni			Ag			Au		
Eo[keV]	Exp.	D & R.	Diff.Model	Exp.	D & R	Diff.Model	Exp.	D & R.	Diff.Model
10	1.180	1.196	1.011	1.398	1.450	1.123	1.750	1.782	1.306
8	1.196	1.221	1.029	1.430	1.510	1.152	1.810	1.910	1.352
6	1.220	1.259	1.056	1.510	1.604	1.184	1.920	2.115	1.396

CuKα

	Al			Ag		
Eo[keV]	Exp.	D & R	Diff.Model	Exp.	D & R	Diff.Model
15	0.800	0.833	-	1.180	1.207	1.115
12	0.775	0.809	-	1.250	1.242	1.176

of the atomic number correction factors derived from $\phi(\rho z)$ curves are much closer to those calculated according to the Duncumb and Reed procedure but tend to be lower by 2 to 10 percent. To determine which atomic number correction factors are most accurate, these corrections were applied to x-ray data from 24 alloy systems measure at low electron energies listed in Table 1. A summary of the results will be found at the end of Chapter VI.

CHAPTER VI

Derivation of the Atomic Number and Absorption Correction

Derivation of the Empirical Formula for $\phi(\rho z)$ Curves

All experimental $\phi(\rho z)$ curves presented in this thesis can be well approximated by an analytical function of the form

$$\phi(R) = DKn(KR)^{n-1} \exp\left[-(KR)^{n}\right] \qquad (6\text{-}1)$$

where $R = \rho z_o + \rho z$, K and n are constants for any curve. This function was chosen since it is found to approximate the $\phi(\rho z)$ curves accurately yet can be integrated to yield the corrections for quantitative analysis. The parameters ρz_o, K and n are obtained by fitting the expression (6-1) using a least squares computer program. With the aid of Eq.(6-1) we have reduced the problem of obtaining $\phi(\rho z, E_o, E_c, Z)$ to the problem of obtaining the parameters $D = D(E_o, E_c, Z)$, $K = K(E_o, E_c, Z)$, $\rho z_o = \rho z_o(E_o, E_c, Z)$ and $n = n(E_o, E_c, Z)$.

Determination of the parameter n

The values of the parameter n obtained by the least squares procedure of the preceding paragraph divided by

the atomic weight A of the matrix element are plotted against the atomic number Z of the matrix element in Fig. 20. The points on this graph represent average values for n for the particular matrix obtained from curves measured at different electron energies and hence different critical excitation energies. The data from individual curves at different electron energies and different critical excitation energies are too close to each other for a particular matrix element (Z) to be plotted separately on the graph. Thus the parameter n depends only on the atomic number and the atomic weight of the matrix element. The solid line of Fig. 20 is obtained from the expression

$$n \doteq \frac{1.95\ A}{Z^{1.32}} \qquad (6\text{-}2)$$

Determination of the parameter K

The logarithms of the values of the parameter K for SiKα and CuKα radiation are plotted versus ln $(E_O - E_C)$ in Fig. 21. This plot yields parallel lines with different slopes for SiKα and CuKα radiation. The expression giving best fit to the values for K was found to be

$$K = \frac{BF}{(E_O - E_C)^m} \qquad (6\text{-}3)$$

where $B = 0.188\ (\frac{1}{E_C})^{1.149}$

$m = (\frac{3.873}{E_C})^{0.3526}$

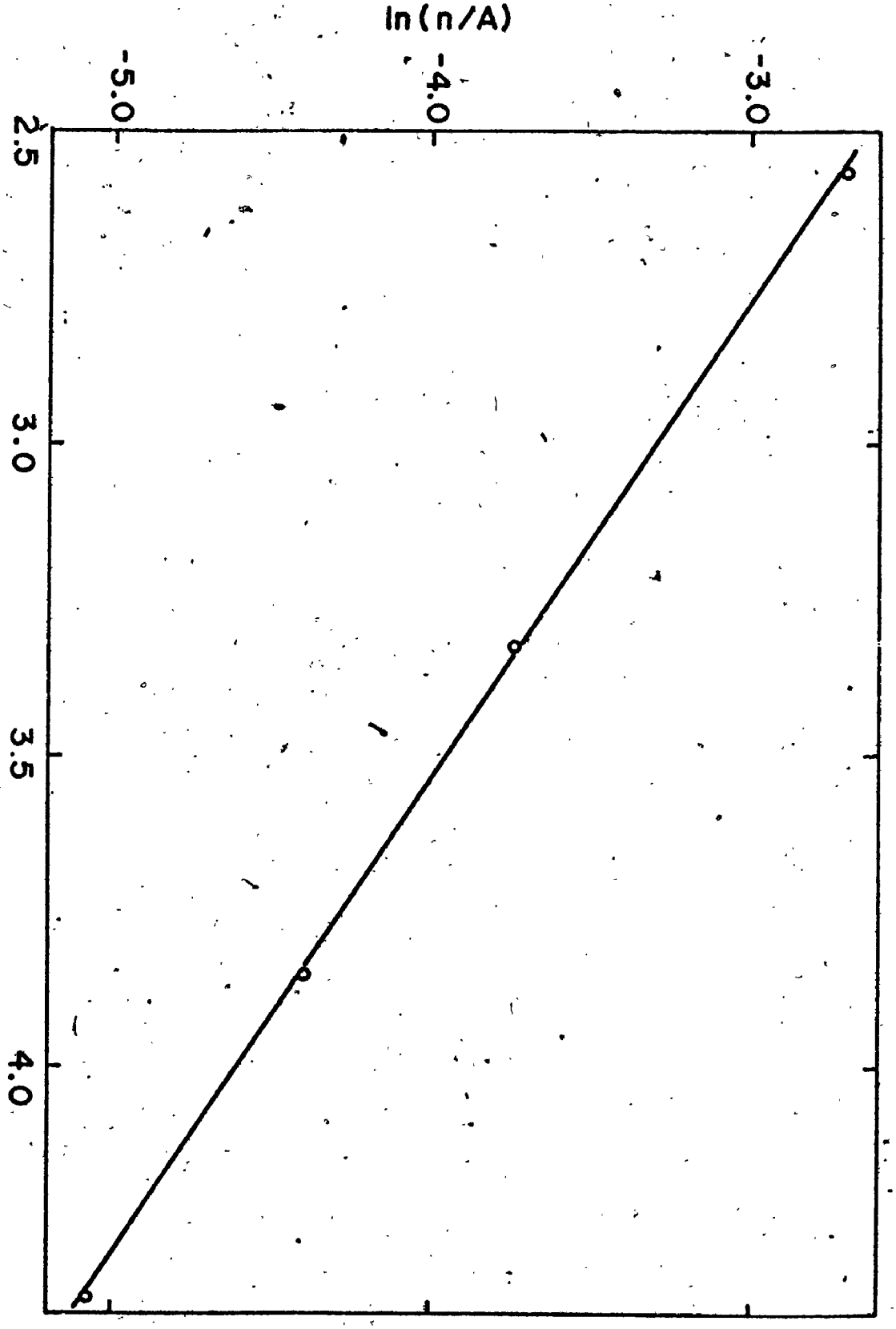

Figure 20. Experimental Data on the Parameter n

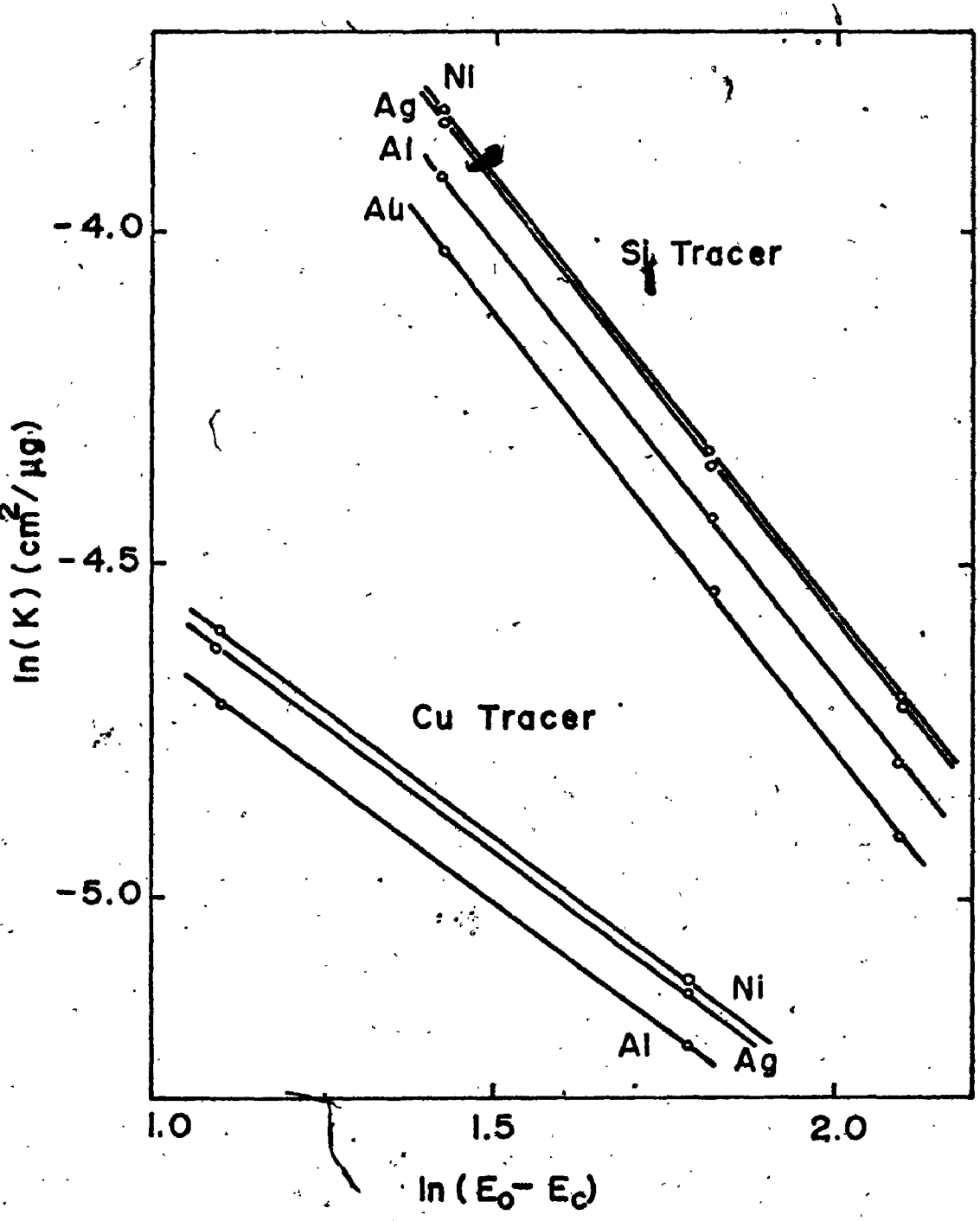

Figure 21. Experimental Data of the Parameter K

and $$F = 1 + 0.0595\ Z^{0.7} / \exp\ (0.00294\ Z^2).$$

Determination of parameter ρz_o

In Fig. 22 the values of the parameter ρz_o are plotted versus energy E_o. This graph indicates that ρz_o is a linear function of electron energy E_o. Further analysis of the slopes of lines reveals that ρz_o depends exponentially on E_c and Z. The equation which fits the values is

$$\rho z_o = (2.571 \times 10^{15}\ E_c)^{0.106}\ E_o\ [\exp\ (0.088\ Z) + 1] / Z^{1.12} \exp\ (0.088\ Z) \qquad (6\text{-}4)$$

Determination of parameter D

The parameter D represents the total area under $\phi(R)$ curve and is related to the atomic number correction. The logarithms of the values of D plotted versus ln $(E_o - E_c)$ are shown in Fig. 23. The slope of the lines increases with decreasing atomic number and increasing critical excitation energy. The parameter D can be calculated from the formula

$$D = Q\ (E_o - E_c)^P \qquad (6\text{-}5)$$

where E_o and E_c are in keV. Parameters Q and P in this formula depend on atomic number Z and critical excitation energy E_c. To obtain the dependence of parameter P,

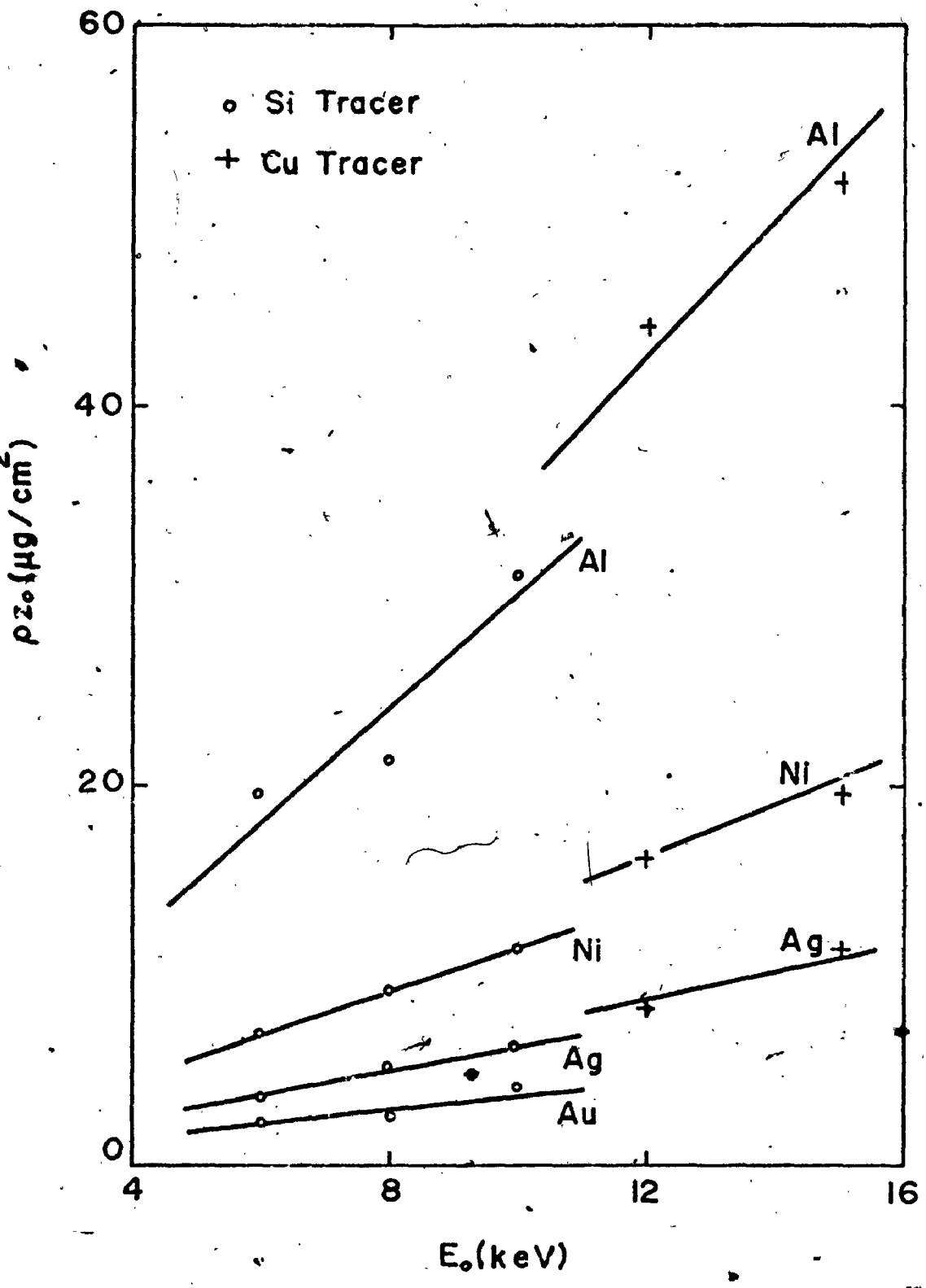

Figure 22. Experimental Data of the Parameter ρz_o

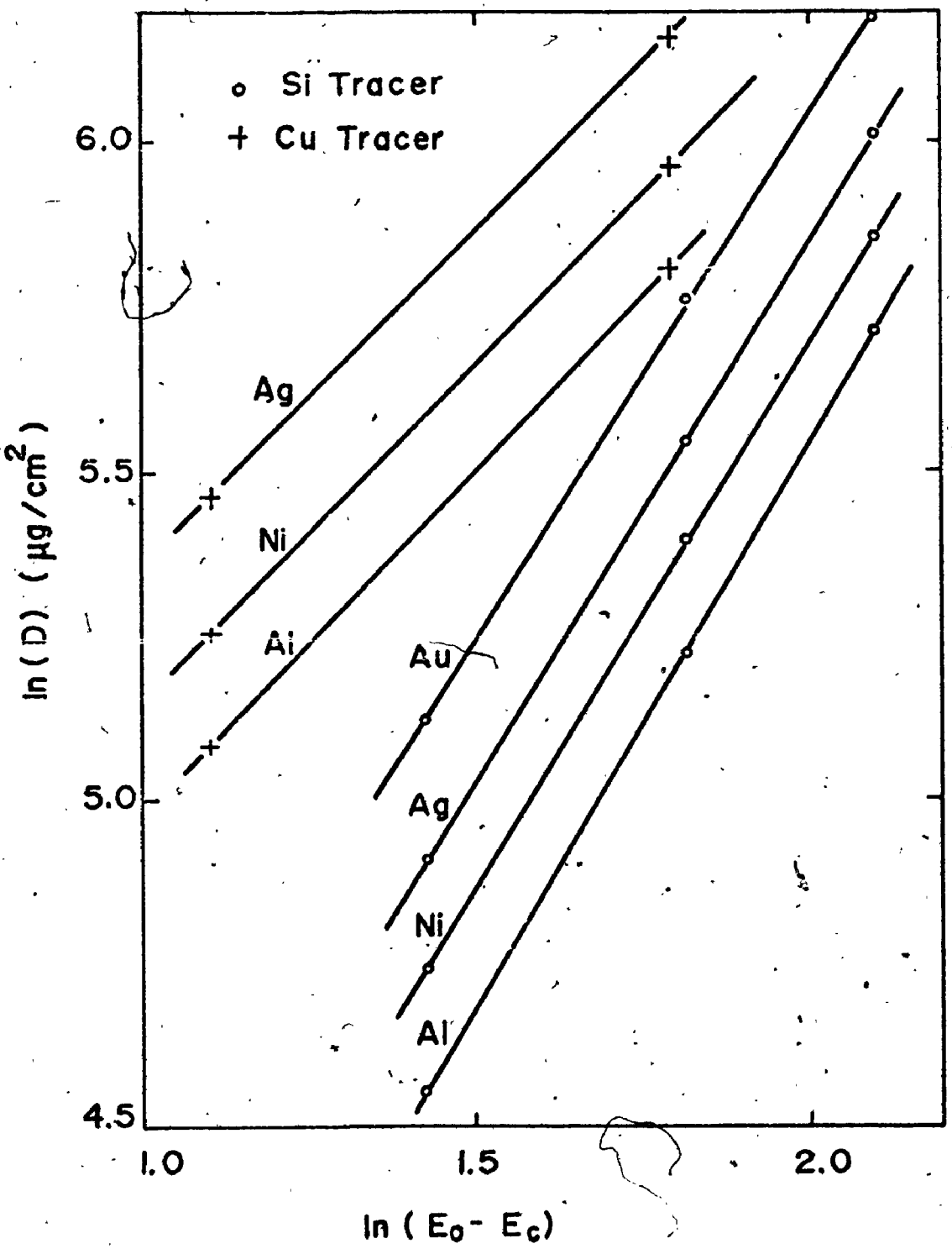

Figure 23. Experimental Data of the Parameter D

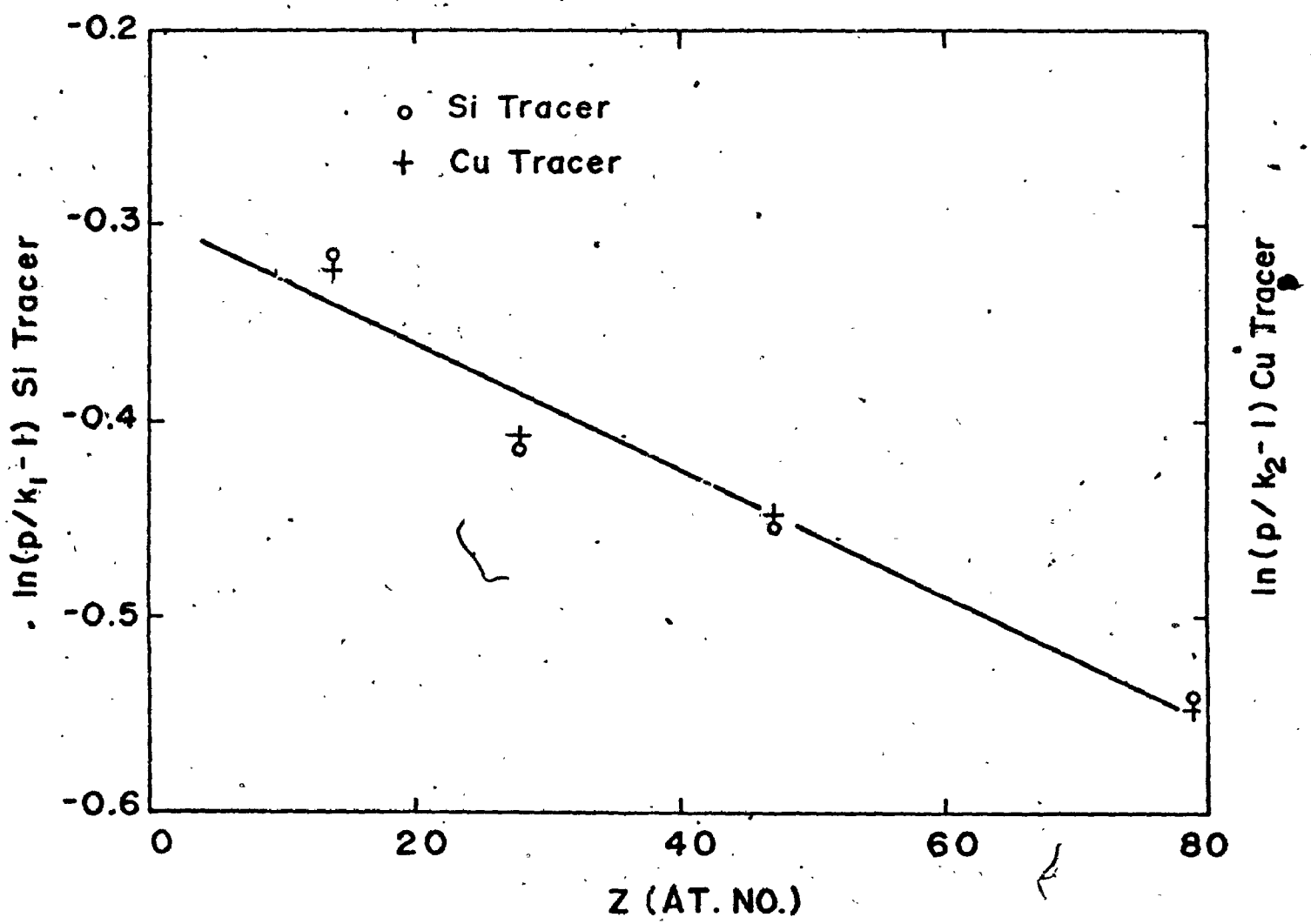

Figure 24. Data of the Parameter P for SiKα and CuKα Radiation

$\ln (\frac{P}{k_1} - 1)$ for SiKα radiation and $\ln (\frac{P}{k_2} - 1)$ for CuKα radiation was plotted versus atomic number Z (Fig. 24). The constants k_1 and k_2 depend on the critical excitation energy. The analytical function which fits the values of P is

$$P = (\frac{1.84}{E_c})^{0.3045} \quad (1 + 0.7417\ e^{-0.00325\ Z}) \qquad (6\text{-}6)$$

The constant 1.84 has the dimensions of energy [keV] since the factor P has to be dimensionless. To calculate the parameter Q, the logarithms of Q was plotted versus atomic number Z (Fig. 25), for both SiKα and CuKα radiation. The result is a line with the slope of 1.135 for both characteristic radiations. The analytical function from which values of Q can be calculated is

$$Q = (3.1245\ E_c)^{1.135} \exp\ (0.0115\ Z) \qquad (6\text{-}7)$$

The Absorption and Atomic Number Correction

With aid of equation (6-1) we can calculate the total intensity emitted by the sample i.e. $G(\chi)$ as

$$G(\chi) = \int_0^\infty \phi(\rho z)\ \exp\ (-\chi\ \rho z)\ d\rho z$$

$$= DK^n n \int_{\rho zo}^{\infty} R^{n-1} \exp\ [-(KR)^n] \exp\ (-\chi R)\ dR \qquad (6\text{-}8)$$

where $\chi = \mu \times \csc \psi$ and μ is mass absorption coefficient and ψ is x-ray take-off angle. Using eq. (6-8) the ratio

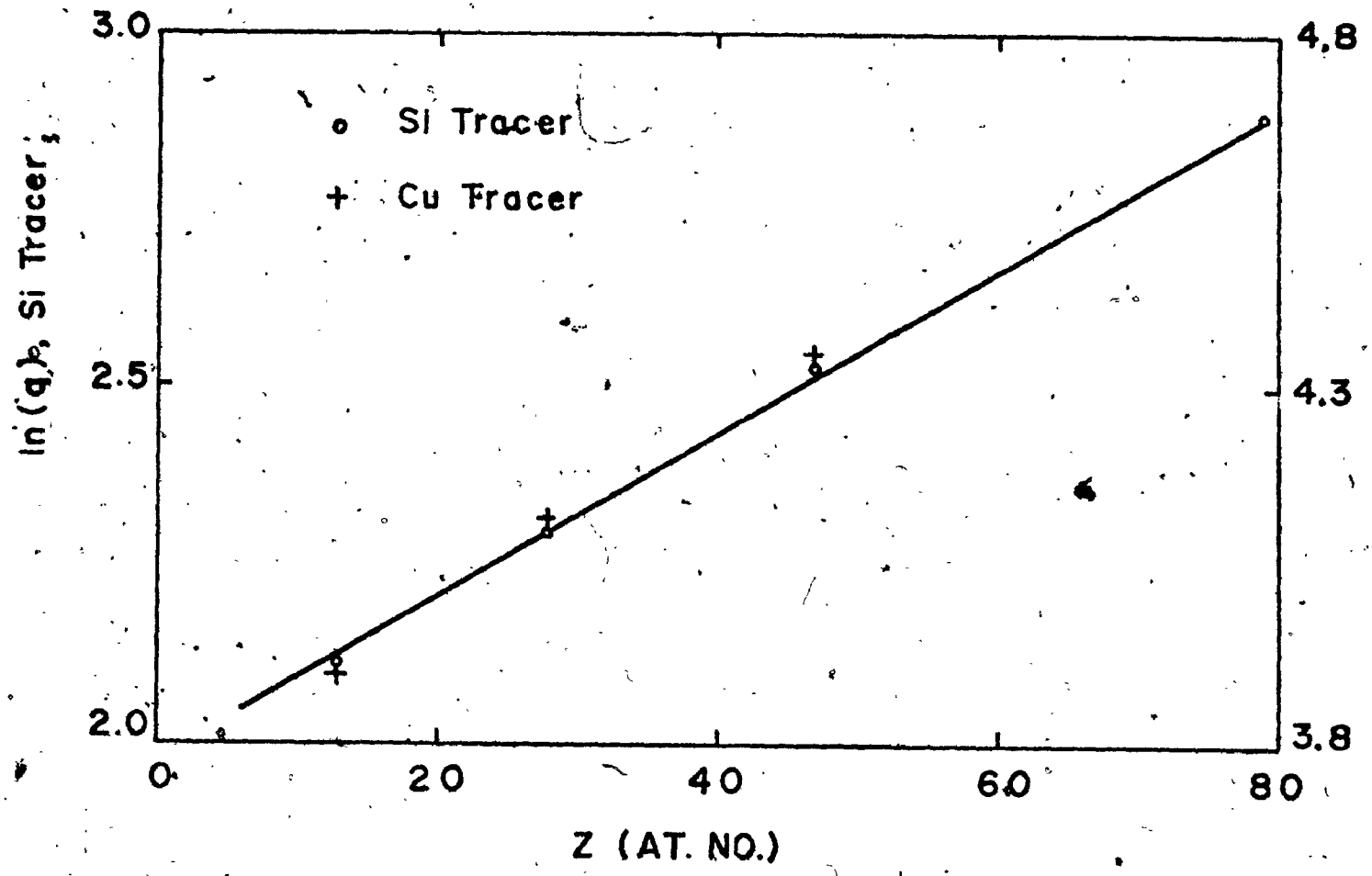

Figure 25. Data of the Parameter Q for SiKα and CuKα Radiation

of the measured x-ray intensity from the specimen to a standard, I_{AB} / I_A, can be written

$$\frac{I_{AB}}{I_A} = C_A \frac{G(\chi)_{AB}}{G(\chi)_A} \qquad (6\text{-}9)$$

where C_A is weight fraction of the element A in AB system. Factors $G(\chi)_{AB}$ and $G(\chi)_A$ can be evaluated from equation (6-8). The factor $G(\chi)_{AB}$ can be calculated under assumption that the atomic number, atomic weight and mass absorption coefficient in equations (6-2), (6-4), (6-6), (6-7) and (6-8) can be replaced by their average values calculated according formulas

$$\bar{Z}_{AB} = C_A Z_A + C_B Z_B$$

$$\bar{A}_{AB} = C_A A_A + C_B A_B$$

and $$\bar{\mu}_{AB} = C_A \mu_A + C_B \mu_B$$

where C_A and C_B are the weight fractions of the elements A and B in the AB system, respectively.

Equation (6-9) was used to calculate the weight concentration for the 24 binary alloys systems of Table 1. Relative errors were calculated from formula

$$\% \text{ rel. errors} = \frac{C_{Cal.} - C_{True}}{C_{True}} \times 100$$

and are shown in Table 15.

To compare results from equation (6-9) with results obtained using the methods of Ziebold and Ogilvie, Belk,

Table 15

Comparison of the Relative Errors Resulting from the Application of the Method Derived in this Thesis and the Methods of Ziebold and Ogilvie, Belk, Thomas, Duncumb and Smith.*

System A-B	Radiation	E_o	True CA	Percent Relative Errors: Present Equation	Z & O	Belk	Thomas	Duncumb	Smith
UAl_2	U-Mα	11	0.815	-1.80	-5.30	-2.90	+1.00	+3.80	-5.60
Ni-Al	Ni-Kα	10	0.421	-0.40	-5.40	-6.80	-1.40	-0.40	+0.20
Ni-Al	"	10	0.592	-1.95	-4.50	-5.50	-2.70	-0.60	-0.90
Fe-Al	Fe-Kα	"	0.408	-1.00	-3.10	-4.20	-2.00	+2.50	+0.50
Ti-Al	Ti-Kα	"	0.372	-5.60	-5.40	-5.00	-11.30	-0.60	-2.20
Fe_2O_3	Fe-Kα	"	0.697	-2.20	+0.50	-2.90	-0.90	+0.50	-1.70
"	"	15	"	-2.30	+1.00	-2.30	-1.10	+0.20	-2.00
Cu-Al	Cu-Kα	12.2	0.041	+4.40	-5.00	+5.60	+0.50	+6.40	+6.80
Al_3Ni	Al-Kα	10	0.579	-0.27	-6.30	+2.20	+7.50	+10.70	+4.10
Al_3Ni_2	"	"	0.408	+3.80	-6.10	+5.10	+15.10	+15.60	+7.70
Al_3Fe	"	"	0.592	+3.40	-3.40	+5.60	+8.40	+11.70	+5.20
Al_3Ti	"	"	0.628	-5.20	-8.40	-2.10	+2.20	-0.10	-3.90
Al_6Mn	"	"	0.747	-2.20	-3.30	+2.50	+3.20	+3.40	+0.40
Al_3Fe	"	"	0.580	+3.00	-7.60	+1.60	+3.90	+4.30	0.00
Al_9Co_2	"	"	0.673	+0.50	-2.80	+5.90	+7.20	+7.60	-3.40
Al_3Ni	"	"	0.580	+1.10	-5.90	+5.90	+8.40	+9.20	+4.40
Al_3Mg_2	"	"	0.624	+2.30	+1.60	-7.10	+6.80	+11.00	+7.90
Al_2Cu	"	"	0.460	+6.30	0.00	+10.50	+17.30	+16.00	+8.60
UC_2	U-Mβ	"	0.908	-0.20	+1.00	-1.60	+1.90	+2.00	-3.70
UN	"	"	0.944	-0.16	+0.40	-1.00	+1.10	+1.20	-2.50
U_3Si	"	"	0.962	+0.05	-0.40	-0.50	+0.80	-0.90	-1.40
UP	"	"	0.885	+0.36	-1.60	-1.70	+2.40	+2.40	-3.30
US	"	"	0.881	+0.20	-2.10	-1.90	+2.10	+2.50	-3.30
U_6Fe	"	"	0.962	+0.73	-0.70	-0.70	+0.40	+0.40	-1.10
Average value and St. dev. =				+0.12±2.8	-2.1±3.7	-0.12±4.6	+3.0±5.9	+4.6±5.2	+0.5±4.2

*Calculated compositions based on experimental data collected by Poole [32].

Thomas, Duncumb, and Smith, the average value and standard deviation for the relative errors were calculated for each method and are shown at the bottom of Table 15. By using the formula developed in this thesis, a considerable reduction in relative error was achieved indicating that a better quantitative correction is obtained for low electron energies.

CONCLUSION

The Depth distribution of the x-ray production, $\phi(\rho z)$ curves have been measured for electron energies below 15keV with electron beam normal to the surface of the specimen for two x-ray energies and 4 matrix elements. All measured $\phi(\rho z)$ curves follow the pattern predicted from the theory of interaction of electrons with atoms of the solid. The curves which have been measured show clearly the changes in the distribution of the x-ray production for a single x-ray energy as the atomic number of the matrix element is changed.

The absorption correction factors, $f(\chi)$ values, calculated from experimental $\phi(\rho z)$ curves are in the range of the $f(\chi)$ values calculated from Philibert formula but $f(\chi)$ values calculated from $\phi(\rho z)$ curves decrease with increasing atomic number for particular electron energy while $f(\chi)$ values calculated from Philibert formula are increasing. This is probably due to the large contribution from continuum. The ratio of the x-ray intensity directly generated by the energetic electrons and by the continuum becomes smaller for low electron energies than for high electron energies.

The atomic number factors calculated from $\phi(\rho z)$ curves are quite different from factors calculated

according the Diffusion Model. Better agreement exists with atomic number factors calculated according to the Duncumb and Reed procedure. An analytical function

$$\phi(R) = nDK^{n}(KR)^{n-1} / \exp(KR)^{n}$$

which describes the depth distribution of the x-ray production as a function of depth, the electron energy, the critical excitation energy and the average atomic number of the specimen was derived. This analytical function approximates well the $\phi(\rho z)$ curves at low electron energies. The parameter n depends only on the average atomic number and atomic weight of the material analyzed but parameter K, ρz_o and D depend on electron energy, critical excitation energy and the average atomic number of the matrix.

The atomic number and absorption corrections developed in this thesis give better agreement for correcting data from standards of known composition at low electron energies than all methods presently in use. This can be seen from the comparison of data of Table 15. The average value of the relative errors for 24 alloy systems calculated according the formula developed in this thesis is 0.12% indicating no bias in the results and the standard deviation of ±2.8% is almost two times smaller than the best previous result. The real advantage of the method developed in this thesis for calculating absorption

and atomic number correction at low electron energies lies in the fact, that calculations are relatively simple. Because this method provides the $\phi(\rho z)$ curve for a particulate substrate, it has potential application in the analysis of film thickness.

Suggestions for Further Work

To extend the work described in this thesis, a new set of sandwich samples suitable for a measurement of $\phi(\rho z)$ curves at low electron energies should be prepared with at least two different tracer elements. The tracer elements should be chosen to provide $\phi(\rho z)$ curves for x-ray radiation in the range of 3 and 5 Å. Measurements should also be made in electron microprobes in which the electron beam is inclined relative to the sample surface. The formula for calculating absorption and atomic number correction developed in this thesis should be extended to data taken at higher electron energies so that a more general correction equation for quantitative analysis is available.

REFERENCES

1. Castaing, R.: Thesis, University of Paris, Onera Publication, No. 55 (1951).
2. Castaing, R. and Descamps, J.: J. Phys. et Radium, 16: 304 (1955).
3. Philibert, J.: in "X-ray Optics and X-ray Microanalysis", (Pattee, H., ed.), Third International Symposium on Microanalysis, SXRM III, p. 379, Academic Press, New York and London (1963).
4. Wittry, D.B.: Thesis, California Institue of Technology (1957).
5. Wittry, D.B.: University of Southern California Engineering Center, USCEC Report, 84-204 (1962).
6. Duncumb, P. and Shields, P.K.: in "X-ray Optics and X-ray Microanalysis", (Pattee, H., ed.), SXRM III, p. 329, Academic Press, New York and London (1963).
7. Henoc, J., Maurice, F. and Kirianenko, A.: Commissariat a l'Energie Atomique - France, CEA Report, 2421 (1964).
8. Reed, S.J.B.: Brit. J. Appl. Phys., 16, 913 (1965).
9. Birks, L.S.: in "Electron Microprobe Analysis", Chapter 9, Wiley, New York (1964).
10. Brown, J.D.: Thesis, University of Maryland (1966).
11. Castaing, R.: Advances in Electronics and Electron Physics, 13: 317 (1960).
12. Archard, G.D. and Mulvey, T.: Proc. 3rd International Symposium on X-ray Microanalysis, Brit. J, Appl. Phys., 14: 626 (1962).

13. Ziebold, T.D. and Ogilvie, R.E.: Anal. Chem., 36: 323 (1964).

14. Theisen, R.: Euratom Report, I-1.

15. Ziebold, T.O. and Ogilvie, R.E.: Anal. Chem., 35: 621 (1963).

16. Thomas, P.M.: Brit. J. Appl. Phys., 14: 397 (1963).

17. Poole, D.M. and Thomas, P.M.: J. Inst. Metals, 90: 241 (1962).

18. Belk, J.A.: Birmingham C.A.T. Tech. Note MET 26 (1964).

19. Green, M.: in "X-ray Optics and X-ray Microanalysis", (Pattee, H., Cosslett, V.E. and Engstrom, A., eds.), Academic Press, p. 361, New York (1963).

20. ibid., p. 59.

21. Bothe, W.: Handbuch der Physik, 24: 18 (1927).

22. Kilipatrick, P. and Hare, D.G.: Phys. Rev., 46; 831 (1934).

23. Archard, G.D.: J. Appl. Phys., 32: 1505 (1961).

24. Wolf, R.C. and Macres, V.G.: in "Electron Probe Microanalysis", (Tousimis, A.J. and Marton, L., eds.), Academic Press, p. 73 (1969).

25. Webster, D.L.: Phys. Rev., 37: 115 (1931).

26. Philibert, J.: J. Inst. Metals, 90: 241 (1961).

27. Tong, M.: Unpublished Work (1961).

28. Theisen, R.: in "Quantitative Electron Microprobe Analysis", Springer-Verlag (1965).

29. Nelms, A.T.: Supplement, NBS Circular, p. 577 (1958).

30. Smith, J.V.: J. of Geology, p. 830 (1965).

31. Green, M.: Proc. 3rd International Symposium on X-ray Microanalysis, Stanford, Academic Press (1962).

32. Poole, D.M.: in "Quantitative Electron Probe Microanalysis", (Heinrich, K.F.J., ed.), National Bureau of Standards Special Publication 298, p. 93 (1968).

33. Heinrich, K.F.J.: in "The Electron Microprobe", Wiley and Sons, p. 664 (1966).

34. Castaing, R. and Henoc, J.: Proc. Symposium on X-ray Optics and Microanalysis. Orsay, France, 120 (1965). (Paris, Herman, 1966).

35. Vignes, A. and Dez, G.: Brit. J. Appl. Phys. (Ser. 2), 1: 1309 (1968).

36. Brown, D.B. and Ogilvie, R.E.: J. App. Phys., 37: 4429 (1966).

37. Brown, D.B. and Wittry, D.B.: presented at the Second National Conference on Electron Microprobe Analysis, Boston (1967).

38. Bethe, M.A., Rose, M.E. and Smith, L.P.: Proc. Am. Phil. Soc., 78: 573 (1938).

39. Berger, M.J.: in "Methods in Computation Physics", Vol. I, p. 135, Academic Press, New York (1963).

40. Archard, G.D. and Mulvey, T.: in "X-ray Optics and X-ray Microanalysis", (Pattee, H., ed.), SXRM III, p. 393 (1963).

41. Worthington, C.R. and Tomlin, S.G.: Proc. Phys. Soc., A69: 401, (1956).

42. Mott, N.F. and Massey, H.S.W.: in "Theory of Atomic Collissions:, Oxford Univ. Press, London and New York (1949).

43. Burhop, E.H.S.: Proc. Cambridge Phil. Soc., 36: 43 (1940).

44. Duncumb, P. and Reed, S.J.B.: in "Quantitative Electron Probe Microanalysis", National Bureau of Standards Special Publication 298, p. 93 (1968).

45. Heinrich, K.F.J.: in "The Electron Microprobe", (McKinley, T.C., Heinrich, K.F.J. and Wittry, D.B., eds.), New York, London and Sydney (1966).

46. Brown, D.B.: Thesis, Massachusetts Institute of Technology (1965).

47. Traill, R.J. and Lachance, G.R.: Geological Survey of Canada Paper, 64-57 (1965).

48. Traill, R.J. and Lachance, G.R.: Canadian Spectroscopy 11, Nos. 2 and 3 (1966).

49. Duncumb, P.: in "1st European Colloquium on Electron Probe Microanalysis" (1964).

50. Heinrich, K.F.J.: Second National Conference on Electron Microprobe Analysis, Boston (1967).

51. Bishop, H.E.: Proc. Phys. Soc. (London), 85: 855 (1965).

52. Murata, K., Shimuzu, R. and Shinoda, G.: Technology Reports, Osaka University, 16: 121 (1966).

53. Shinoda, G., Murata, K. and Shimuzu, R.: in "Quantitative Electron Proble Microanalysis", National Bureau of Standards Special Publication 298, p. 155 (1968).

54. Duncumb, P. and Shields, P.K.: Brit. J. Appl. Phys., 14: 617 (1963).

55. Brown, J.D.: Advances in Electronic and Electron Physics, Supplement 6 (1969).

56. Brown, J.D. and Parobek, L.: X-ray Optics and Microanalysis, Tokyo (1972).

57. Schmitz, U., Ryder, P.L., and Pitsch, W.: Vth Int. Congress of X-ray Optics and Microanalysis, Berlin, p. 104 (1968).

58. Bishop, H.E.: X-ray Optics and Microanalysis (Herman, Paris) p. 112 (1966).

59. Goudsmit, S. and Saunderson, J.L.: Phys. Rev. 57, 24 (1940).

60. Nigam, B.P., Sundaresan, M.K. and Wu, Y.T.: Phys. Rev. 115, p. 491 (1959).

61. Hutchins, G.A.: Second National Conference on Electron Microprobe Analysis, Boston, Mass. (1967).